Interceptor Guidance Using Angle-only Measurements and Discrete Maneuvers

by

Anthony John Bogner
B.S.A.E., Texas A & M University
(1987)

Submitted in Partial Fulfillment
of the Requirements for the
Degree of
Master of Science
in Aeronautics and Astronautics
at the
Massachusetts Institute of Technology
June, 1990

Signature of Author _____
Department of Aeronautics and Astronautics
June, 1990

Certified by _____
Professor Richard H. Battin
Department of Aeronautics and Astronautics
Thesis Supervisor

Certified by _____
Richard E. Phillips
Technical Supervisor, CSDL

Accepted by _____
Professor Harold Y. Wachman
Chairman, Departmental Graduate Committee

Interceptor Guidance Using Angle-only Measurements and Discrete Maneuvers

by

Anthony J. Bogner

Submitted to the
Department of Aeronautics and Astronautics
on May 22, 1990 in partial fulfillment of the requirements
for the Degree of Master of Science.

Abstract

A guidance algorithm for a long-range interceptor that: (1) takes angle-only measurements of the target and, (2) performs only discrete maneuvers is developed and studied. The algorithm enhances the information content of the navigation filter by 'linking' guidance trajectory selection and navigation filter performance. The guidance algorithm calls for the minimization of a quadratic cost function composed of two terms—variance in time-to-go and fuel usage. The first term, variance in time-to-go at the end of all target tracking, provides a measure of navigation filter performance, while the second term, fuel usage, provides a measure of the two discrete velocity corrections used to enhance navigation filter performance.

The performance and behavior of the guidance algorithm were examined for several different target-interceptor closing trajectories. For all trajectories, the guidance algorithm achieved about the same final standard deviation in time-to-go (ie. standard deviation at intercept). However, to achieve this, the magnitude of the velocity corrections varied considerably between trajectories. In the short missions, the second maneuver was substantially larger than the first, but in the long missions, the first maneuver was substantially larger than the second. The factor driving this variation between intercept trajectories is the closing speed of the interceptor relative to the target. The final state uncertainty in the navigation filter was also trajectory dependent, with the longer missions achieving a slightly lower state uncertainty at intercept than the shorter missions.

Thesis Supervisor: Dr. Richard H. Battin

Title: Adjunct Professor of Aeronautics and Astronautics

Technical Supervisor: Richard E. Phillips

Title: Section Chief, The Charles Stark Draper Laboratory, Inc.

Acknowledgements

This thesis has been made possible through the academic and personal support of many people. In response to this support, I would like to thank all those who have helped make both this thesis possible and my time here at MIT and Draper Laboratory so rewarding.

Thank you Tim Brand, for the opportunity to perform graduate work here at Draper Laboratory and for the interesting summer work that has made these last two summers go by much too fast. Special thanks to Dr. Richard Phillips, my Technical Supervisor at the Charles Stark Draper Laboratory, for the technical expertise that he has continually shared with me. His constant availability for questions as well as his insight and guidance have been truly invaluable. Special thanks also to Dr. Richard Battin for his assistance in the preparation of this thesis and his teaching in the field of Astrodynamics. It has certainly been my privilege to be one of his students.

Many others at Draper have contributed to my rewarding educational experience. My officemate, Todd Dierlam, has been one of the finest persons to have shared this experience with. The comradery and friendship (as well as the late nights and weekends at the lab) have made these two years much more enjoyable. If I decide to do it again, I won't hesitate to give you a call! The same goes for Craig Niiya, fellow Draper Fellow. The friendship (and appreciation of mathematical rigor) that we've shared in our academic and personal lives will not be forgotten. Thanks also to Peter Millington (Gig'em Ag's), Ron Simmons, Ralph Galetti, and the rest of the Draper Fellows. Your friendship has made my stay here in Boston a great one.

I would like to express my appreciation to the TCC crew—Mark M., Mark V., Bill, Dan, Chris, Lupe, and Paula. Our discussions and interaction have made my spiritual and personal life more complete. (You guys also supplied me with a terrific excuse to get out of the Lab and take the needed study breaks!) Joking aside—All the best!

Mom, Joe, and Grandma—thank you for being the terrific family that you are. I am truly grateful for the support that you all have given me during my entire education. I dedicate my education to you.

Finally. Thank you Paula. The time we have shared here at MIT has been more than special. May there be more.

This report was prepared at The Charles Stark Draper Laboratory, Inc. under Navy Contract N00030-84-C-0036.

Anthony J. Bogner

Contents

List of Figures

List of Tables

List of Symbols

Symbol	Description
$\vec{a}_g$	Acceleration due to gravity
C	Partial of angle measurement sensitivity, h, with respect to state, x
$\mathrm{E}\{\cdot\}$	Expected value
f	Weight factor for variance in time-to-go
$\vec{F}$	Force
h	Angle measurement sensitivity to state
J	Value of cost function
K	Kalman gain matrix
m	Partial of time-to-go with respect of state, x
m_i	Mass of interceptor
m_t	Mass of target
P	State covariance matrix
$\vec{r}$	Position vector of interceptor relative to target
$\vec{r}_i$	Inertial position vector of interceptor
$\vec{r}_t$	Inertial position vector of target

S	State information matrix, equal to inverse of covariance matrix
t	Time
t_{go}	Time-to-go
u	Six element vector containing velocity impulses
$\mathrm{U}(t)$	Unit step function
v	Magnitude of $\vec{v}$
$\vec{v}$	Velocity vector of interceptor relative to target
w	Vector containing angle measurement noise components, w_θ and w_ϕ
w_θ	Gaussian random noise corrupting azimuth measurement
w_ϕ	Gaussian random noise corrupting elevation measurement
W	Covariance matrix of random noise, w.
x	Six element state vector containing both position and velocity
XYZ	Inertial Coordinate Frame
xyz	Target-centered coordinate frame
y	Two element vector containing equivalent measured angles θ and ϕ
$\delta(t)$	Delta function
ΔV	Six element vector composed of ΔV_1 and ΔV_2
ΔV_1	Vector containing first velocity impulse
ΔV_2	Vector containing second velocity impulse
$\Delta V_3 = \Delta V_{hit}$	Vector containing final velocity impulse
θ	Equivalent azimuth angle in target-centered coordinates

θ'	Azimuth angle measured by interceptor
μ	Earth gravitational constant
σ	Standard deviation
σ^2_{tgo}	Variance in time-to-go
ϕ	Equivalent elevation angle in target-centered coordinates
ϕ'	Elevation angle measured by interceptor
$\vec{0}$	Three element zero vector
$0_{3\times3}$	Three by three zero matrix
$I_{3\times3}$	Three by three identity matrix

Subscripts

true	Values measured with no noise
nh	No hit maneuver performed

Superscripts

$\wedge$	Navigation filter estimate
$+$	New value (after measurement update)

– Old value (before measurement update)

Chapter 1

Introduction

The purpose of this investigation is to develop and study a guidance algorithm for a long-range interceptor that takes angle-only measurements of the target. The guidance design philosophy is to have the guidance algorithm select an intercept trajectory which enhances or maximizes the information content of the navigation filter.

To motivate this design philosophy, consider the implied objective of any interceptor guidance—to cause the interceptor to hit or come as close as possible to the target at a specified hit-time. For the non-evasive target, this objective requires that the interceptor have both a good dynamics model to predict target behavior and a navigation filter with a high quality estimate of the target state (ie. position and velocity). The first of these requirements can be met by understanding and modeling the forces causing the target motion. In this study, the target is assumed to be in low earth orbit where gravitational forces are understood and predictable to high accuracy. The second requirement can be met by having the guidance work with the navigation filter to enhance measurement observability, while at the same time pro-

ducing an intercept in a reasonable amount of time. Intuition suggests that the two elements of this second requirement become a trade-off. An interceptor that focuses only on enhancing measurement observability, with no terminal condition requiring intercept, would likely perform maneuvers that allow the navigation filter to "look at" the target from many different perspectives in an effort to accurately determine the state of it's target. Such maneuvering would require a prohibitively large amount of fuel and time. At the other extreme is the interceptor that continuously heads straight for the target, providing the filter with little or no measurement observability.

In an effort to strike a balance between measurement observability and getting the interceptor to the target in a reasonable amount of time, the guidance in this study "links" fuel usage and navigation filter performance together in a quadratic cost function. Using the variance in time-to-go as a measure of navigation filter performance, the guidance attempts to minimize the cost function, allowing a trade-off between fuel usage and variance in time-to-go.

In order to motivate the selection of these two terms for the cost function and further explain the cost function formulation being proposed, the following sections provide background assumptions about the nominal mission profile as well as review previous work in the area of angle-only guidance. Section 1.1 begins with a summary of the capabilities and limitations of the interceptor and target. Section 1.2 then incorporates the constraints into a nominal mission profile and, in conjunction with Section 1.1, defines the problem to be solved. Section 1.3 reviews previous work in the area of angle-only guidance as a background to the guidance design being presented

here. Finally, in Section 1.4, the proposed guidance is summarized.

1.1 Target and Interceptor Constraints

As with the design of most interceptors, operational considerations such as safety, maintenance, and tactics place restrictions not only on the types of hardware used onboard the interceptor, but also on its mission profile. The interceptor being examined here is no exception. Operational considerations place three unusual constraints on this interceptor—constraints that affect guidance design.

The first constraint, which stems from safety and maintenance considerations, requires the interceptor divert system to use solid propellants, rather than liquid propellants, as the primary means of thrust. Because of this, divert maneuvers will consist of staged, midcourse-corrections rather than continuous divert accelerations.

The second constraint concerns the type of target tracking system and the periods during which it can be used to perform the tracking function. First, a passive type device will be used to supply angular measurements of the target. This serves to keep the sensor less complex than an active device and prevents the interceptor from announcing its presence to the target. Second, because of the midcourse-correction style guidance, coast periods will exist between successive divert maneuvers. By restricting target tracking to these coast periods, angle measurements can be made in a relatively vibration free environment and, thus provide high-quality angle measurements of the target.

These coast periods will provide a relatively vibration-free environment for target

tracking. Thus, restricting the measurements to these short coast periods will ensure high-quality angle measurements of the target.

The third constraint requires the interceptor to complete all maneuvers before intercept so that performance of the fusing mechanism is not degraded. The fusing mechanism is a kill enhancement device consisting of tethered masses which extend to increase the possible area of contact. This device can not be deployed during powered flight.

Finally, in addition to the interceptor operational considerations just mentioned, a brief comment is necessary concerning the maneuvering capabilities of the target. For this study, the target is assumed to be in a low earth orbit with little or no maneuvering capability. This will prevent the target from performing evasive maneuvers, even if it detects the interceptor's intent.

1.2 Nominal Mission Profile

Given the constraints of Section 1.1, the following nominal mission profile was developed and is depicted in Figure 1.1. The mission starts on the ground where the interceptor is given an estimate of the target's state. Using this relatively low quality estimate, the interceptor is sent toward the target, entering the period of the mission typically referred to as the *boost phase.* The boost phase ends when the interceptor exits the sensible atmosphere and reaches a range of approximately $1,000$ km from its target. At the end of the boost phase, the interceptor enters a coast period during which it proceeds to take measurements of the target. The beginning of this

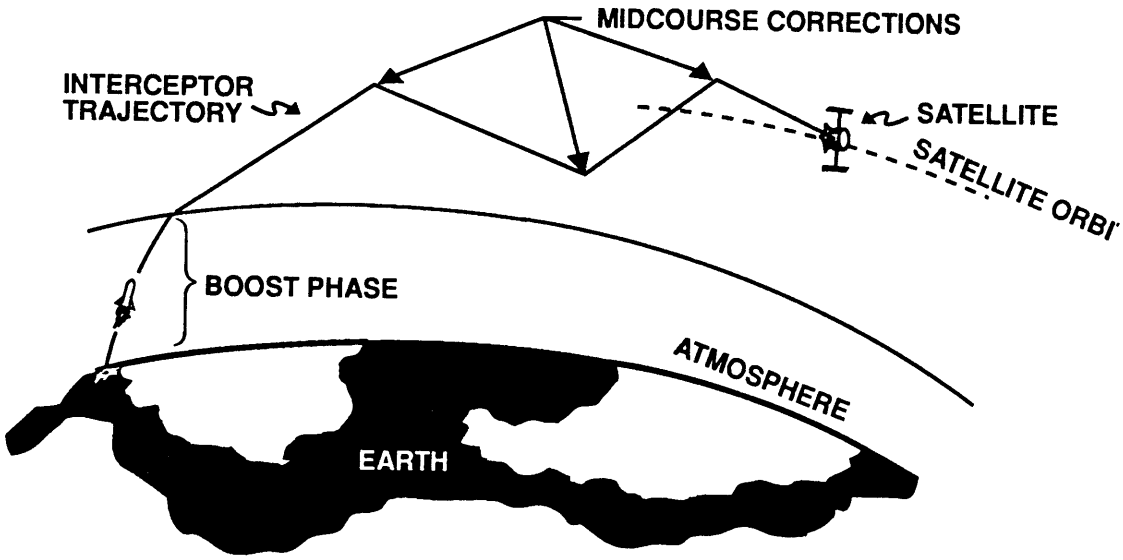

Figure 1.1. Nominal Mission Profile

measurement period marks the start of the guidance design considered here.

The guidance problem begins with the conditions of the target and interceptor at the start of the measurement period. These conditions include position and velocity as well as their respective uncertainties as given by the state covariance matrix. Because the interceptor takes no measurements during the boost phase, the quality of the target state (position and velocity) estimate remains low.

As the interceptor proceeds toward its target, angle measurements are processed by the navigation filter (a discrete Kalman filter) to improve the quality of the target state estimate. At the end of the measurement period, the guidance determines a set of maneuvers (ΔV_1, ΔV_2, and ΔV_{hit}) which will enhance the information content of the navigation filter as well as provide for target intercept. The first maneuver, ΔV_1, is applied immediately. The second and third maneuvers, ΔV_2 and ΔV_{hit}, are predicted by the guidance but will be recomputed and applied later in the trajectory. This prediction, however, allows the guidance to anticipate the application of maneuvers later in the trajectory.

After applying the first maneuver, the interceptor enters a second coast period during which measurements are taken. At the end of this second measurement period, the second and third maneuvers (ΔV_2 and ΔV_{hit}) are recomputed. After applying the second maneuver, ΔV_2, the interceptor enters its last measurement period. At the end of this period, the guidance computes and applies the velocity change necessary to intercept the target at the scheduled time. The entire mission time-line is summarized in Figure 1.2.

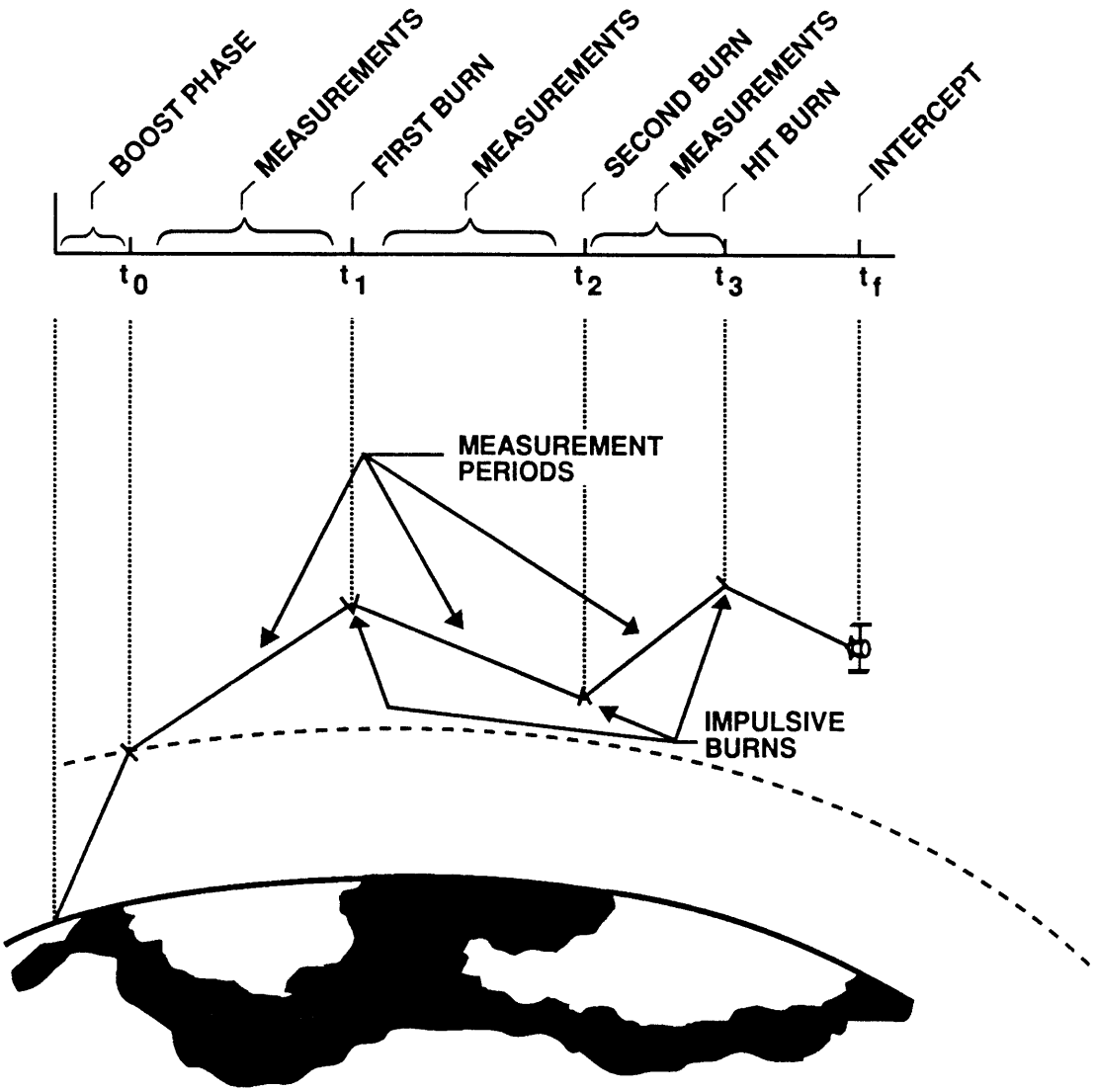

Figure 1.2. Mission Time-Line

1.3 Previous Work

Much work has been devoted to the use of angle-only measurements in solving the interceptor guidance problem. Early research in this area focused on using angle measurements for the direct determination of guidance commands. That is, no attempt was made to obtain information from the angle measurements in order to increase the interceptor's knowledge about the complete state (position, velocity) of the target. The guidance law resulting from this research and having the characteristics just cited is called *proportional navigation.* In proportional navigation, the interceptor continually monitors two inertial angles to the target, namely azimuth and elevation. If these angles start changing, the interceptor generates vehicle accelerations that prevent the change, or null the line-of-sight rate. This approach ensures that the interceptor will hit the target but at an unspecified time. Such a guidance law will not be useful for the problem at hand since this interceptor can not be thrusting through the target at the time of intercept.

Later research focused on deriving information about the state of the target from the angle measurements through the use of an extended Kalman filter in cascade with, but independent of, the guidance law. Such guidance laws made no effort to increase the quality of information in the filter but focused only on getting the interceptor to the target, leaving the filter to do its best along the nominal trajectory. The performance of this type of guidance law was examined by Speyer and Hull [1]. In Ref [1], Speyer and Hull compare different extended Kalman (navigation) filter formulations using an "ad hoc" guidance law in all formulations. The "ad hoc"

guidance law involved a quadratic cost function with no terms specifically dependent on filter performance. They found that filter observability was reduced because the guidance law attempted to null the line-of-sight rate, very much like proportional navigation. They concluded that navigation filter and guidance system design should not be separated and that the guidance should "... perform so as to enhance the filter observability". Thus, as guidance laws matured, the guidance started to work with the navigation filter so as to enhance the information content of the filter.

Various approaches have been taken to achieve this result. In Ref [2], Speyer et al. develop a guidance algorithm that uses numerical optimization to maximize a performance index. The performance index is taken to be the trace of the information matrix at the time of intercept. The resulting trajectory indicates that the azimuth and elevation angles should be kept in motion to increase filter observability. In order to achieve the resulting optimal trajectory, however, the interceptor would likely require continuous divert-maneuvering capability that is not available to the interceptor being considered here.

An algorithm more suited to the constraints of this interceptor is that developed by Casler [3]. In Ref [3], Casler presents a guidance algorithm that attempts to "... minimize or substantially reduce the terminal variance" in some specified guidance parameter. For his study, guidance performance was evaluated using three different guidance parameters, namely: (1) miss (distance of closet approach), (2) final velocity change required for intercept, and (3) time-to-go. Prior to the analysis Casler predicted that the best choice for the guidance parameter was time-to-go

since "nonlinear filter convergence and guidance calculations hinge on the estimate of time-to-intercept." This was verified in his analysis. This result, as well as the current mission requirement for a terminal coast period, provide motivation for the selection of variance in time-to-go as one of the components of the quadratic cost function being presented here.

One unattractive feature of Casler's algorithm is the "minimization" of the terminal variance. Rather than performing a true minimization, the algorithm actually performs a gradient search to the point of diminishing returns. Casler states that "although a large velocity correction introduces a larger measurable line-of-sight rate, it may not improve estimation accuracy significantly, ...". By incorporating fuel usage into the cost function proposed here, a true minimum is introduced and an arbitrary decision about what contribution is considered "significant" is avoided.

1.4 Guidance Approach

With this review of interceptor constraints and previous work as a starting point, the following guidance was developed. The guidance law calls for the minimization of a quadratic cost function containing two terms:

- variance in time-to-go, σ^2_{tgo}, at the end of the last measurement period, and
- the square of the magnitude of all velocity corrections.

The selection of the first term is motivated by the results of Casler as well as a consideration of the terminal-coast condition. Since the interceptor must not be thrusting on impact, a high quality estimate of time-to-go is important. The selection

of the square of the magnitude of all velocity corrections is motivated by a need to limit fuel requirements. As suggested earlier, neglecting fuel usage in the cost function would likely produce trajectories that require prohibitively large velocity changes.

With the components of the cost function presented, it is now appropriate to write a mathematically expression for the entire cost function. Letting J represent the value of the cost function gives

$$J = \frac{1}{2} \sum_{i=1}^{3} |\Delta V_i|^2 + f\, \sigma_{tgo}^2 \Big|_{t=t_3} \tag{1.1}$$

where:

$$\begin{aligned} f &= \text{weight factor for variance in time-to-go} \\ t_3 &= \text{time right before final hit maneuver} \end{aligned}$$

The objective of the guidance is to minimize J. Minimization of the cost function is performed by selecting ΔV_1 and ΔV_2. The final maneuver, ΔV_{hit}, must be such that the interceptor hits the target at the desired time. This is not selectable, but rather fixed by the physics of the situation.

Notice that a weight factor, f, is included for the variance term to allow for scaling of the term to the same order of magnitude as the fuel usage. It is this weight factor that allows overall cost function minimization to become a trade-off between σ_{tgo}^2 and fuel usage. By making the weight on variance relatively large, the guidance will put more emphasis on reducing σ_{tgo}^2 at the expense of larger velocity corrections. The opposite effect can be achieved by making the weight relatively small and accepting a larger variance in time-to-go. This weight factor essentially becomes a design tool,

allowing the guidance designer the flexibility to control which quantity the guidance will place more emphasis on when minimizing the cost function.

With the objective of the guidance algorithm outlined, it now becomes necessary to expand on the computation of J. Chapter 2 outlines the formulation of σ^2_{tgo} and the rest of the cost function starting with the definition of the coordinate systems and dynamics model used to simulate interceptor behavior. Chapter 3 then outlines the minimization of the cost function.

Chapter 2

Proposed Guidance

With the components of the cost function presented in Chapter 1, it is now appropriate to expand on the computation of each component. Following a logical progression to that end, this chapter proceeds by first developing the guidance state and measurement equations in Sections 2.1. Then, in Section 2.2, the guidance model used to predict navigation filter performance is presented. Section 2.3 and 2.4 summarize the equations necessary to compute each component of the cost function. Finally, in Section 2.5, the equations for each component are combined to give an expression for the total cost function.

Because the guidance algorithm is a "predictor", taking the conditions (states and uncertainties) at the current time and predicting each of the components of Equation 1.1, close attention must be paid to initial conditions throughout the development of the guidance equations. It is certainly true that the initial conditions do not change the theory behind the algorithm, but they do contribute to the notational complexity. This is because the initial conditions for all equations in the guidance depend on

which velocity corrections have or have not, been applied.

2.1 Guidance State and Measurement Equations

This section details the coordinate systems, equations of motion, and measurement equations used in the guidance algorithm. Although two simplifying assumptions are made in the development of the guidance algorithm, its performance is assessed in a more realistic environment.

2.1.1 Coordinate System and Equations of Motion

The equations of motion for the interceptor were cast in a target-centered coordinate system. To develop the equations of motion in this frame, consider the target-interceptor geometry depicted in Figure 2.1. Let XYZ denote an inertially fixed frame and xyz denote a non-rotating, target-centered frame whose coordinate directions are parallel to XYZ's. If the position of the interceptor and target in the inertial frame are $\vec{r}_i$ and $\vec{r}_t$ respectively, then the position, $\vec{r}$, of the interceptor relative to the target is given by

$$\vec{r} = \vec{r}_i - \vec{r}_t \tag{2.1}$$

Taking two time derivatives produces a vector differential equation in position, namely

$$\ddot{\vec{r}} = \ddot{\vec{r}}_i - \ddot{\vec{r}}_t \tag{2.2}$$

By examining the forces acting on the interceptor, the inertial derivatives, $\ddot{\vec{r}}_i$ and $\ddot{\vec{r}}_t$, can be related to the velocity corrections.

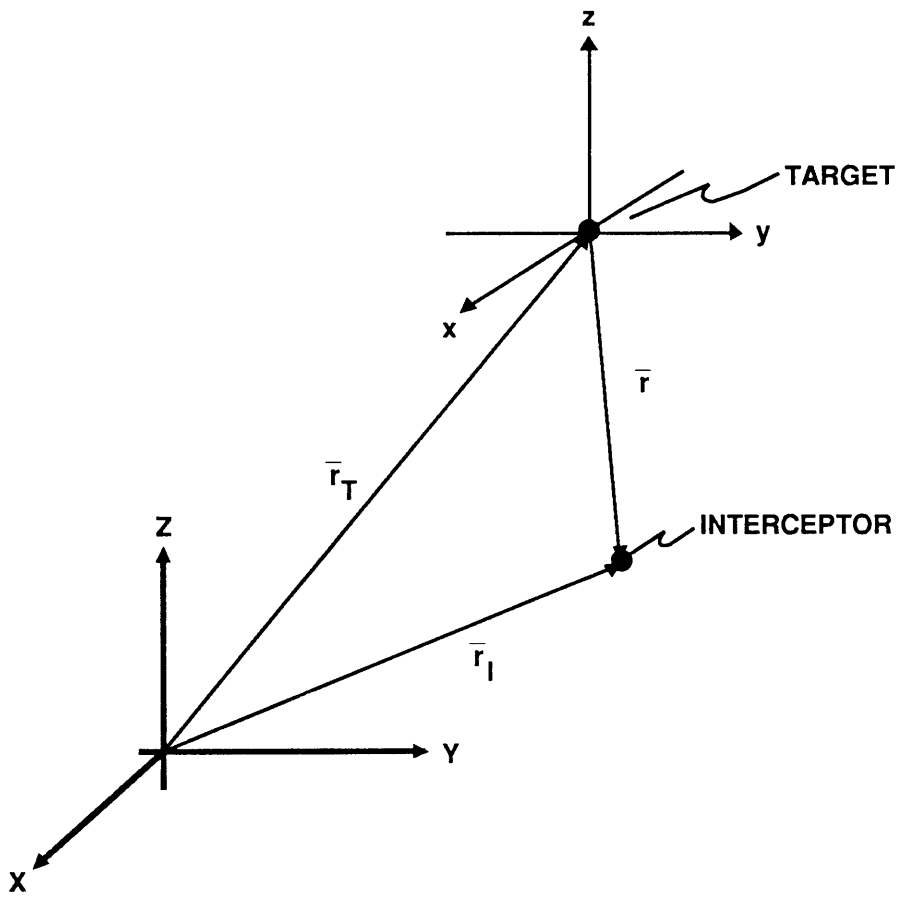

Figure 2.1. Typical Target-Interceptor Geometry

For modeling purposes in the guidance algorithm, the following assumptions are made.

- Gravity is the only force acting on both vehicles, each experiencing the same gravitational acceleration, $\vec{a}_g$.
- The interceptor receives three impulsive velocity changes, two for measurement enhancement (ΔV_1 and ΔV_2) and one for interception (ΔV_{hit}).

Consideration of the expected engagement time and the proximity of the two vehicles form a basis for the first assumption. Although the target and interceptor experience slightly different gravitational accelerations, the interceptor will have completed its mission within 100–200 seconds, allowing gravity little time to 'curve' the relative trajectory. The second assumption, that the velocity changes are applied as impulses, involves a modeling decision. Non-impulsive maneuvers would, to some extent, reduce both the total observation time and the trajectory deviations that the guidance is trying to induce. However, this assumption, as well as the first, is not critical to the "proof of principle" that is being demonstrated here. In fact, it is likely that both of these assumptions would be retained for an operational algorithm. Any loss of predicted observability resulting from these assumption, if significant, could easily be compensated for by a slight adjustment in the cost function weighting factor.

With these assumptions, a sum of forces on both the target and interceptor produces

$$\sum \vec{F}_i \implies m_i \left[\sum_{i=1}^{3} \Delta V_i \delta(t - t_i) + \vec{a}_g \right] = m_i \ddot{\vec{r}}_i \tag{2.3}$$

$$\sum \vec{F}_t \implies m_t \vec{a}_g = m_t \ddot{\vec{r}}_t \tag{2.4}$$

where

ΔV_i = represents the i^{th} velocity correction

t_i = time that i^{th} velocity correction is applied

Canceling the mass term on each side of Equation 2.3 and 2.4 and substituting the resulting expressions for $\ddot{\vec{r}}_i$ and $\ddot{\vec{r}}_t$ into Equation 2.2 produces the equation of motion of the interceptor relative to the target.

$$\ddot{\vec{r}} = \sum_{i=1}^{3} \Delta V_i \delta(t - t_i) \tag{2.5}$$

This can be written in state space form as

$$\dot{x} = Ax + u \tag{2.6}$$

where

$$x \equiv \left\{ \begin{array}{c} \vec{r} \\ \dot{\vec{r}} \end{array} \right\} \tag{2.7}$$

$$u \equiv \left\{ \begin{array}{c} \vec{0} \\ \sum_{i=1}^{3} \Delta V_i \delta(t - t_i) \end{array} \right\} \tag{2.8}$$

$$A \equiv \left\{ \begin{array}{cc} 0_{3\times3} & I_{3\times3} \\ 0_{3\times3} & 0_{3\times3} \end{array} \right\} \tag{2.9}$$

From Equation 2.5 it is possible to determine closed-form expressions for both position and velocity as functions of time. Performing two integrations produces the equations of Table 2.1. Notice that different expressions are obtained based on the time at which the guidance algorithm is exercised (or called). For example, if the guidance is called prior to the first maneuver, ΔV_1, then this first maneuver must be

Table 2.1. Equations of Motion for Various Guidance Call Times

Guidance Called at t_g	Equations of Motion
$t_0 \leq t_g < t_1$	$\vec{r}(t) = \vec{r}(t_g) + (t - t_g)\,\vec{v}(t_g) + \sum_{i=1}^{3}(t - t_i)\,\Delta V_i\,\mathrm{U}(t - t_i)$ $\vec{v}(t) = \vec{v}(t_g) + \sum_{i=1}^{3}\,\Delta V_i\,\mathrm{U}(t - t_i)$
$t_1 \leq t_g < t_2$	$\vec{r}(t) = \vec{r}(t_g) + (t - t_g)\,\vec{v}(t_g) + \sum_{i=2}^{3}(t - t_i)\,\Delta V_i\,\mathrm{U}(t - t_i)$ $\vec{v}(t) = \vec{v}(t_g) + \sum_{i=2}^{3}\,\Delta V_i\,\mathrm{U}(t - t_i)$
$t_2 \leq t_g < t_3$	$\vec{r}(t) = \vec{r}(t_g) + (t - t_g)\,\vec{v}(t_g) + (t - t_i)\,\Delta V_3$ $\vec{v}(t) = \vec{v}(t_g) + (t - t_3)\Delta V_3$

included in the formulation. However, after this maneuver has been applied, ΔV_1 is no longer included in the equations but is accounted for in the initial conditions.

The several equations of Table 2.1 can be reduced to two if a new variable is introduced—namely, the time, t_g, at which the guidance call is made. The equations of Table 2.1 then reduce to the slightly more complicated expressions of Table 2.2. The second unit step introduced in these equations permits the guidance equations to "know" which velocity corrections have, or have not, occurred.

2.1.2 Measurement Equations

The actual angle measurements taken by the interceptor are made in an interceptor-centered coordinate frame whose axes are parallel to the target-centered axes, xyz. The interceptor will measure the azimuth and elevation angles, θ' and ϕ', indicated

Table 2.2. Simplified Equations of Motion for Various Guidance Call Times

Guidance Called at t_g	Equations of Motion
$t_0 \leq t_g < t_3$	$\vec{r}(t) = \vec{r}(t_g) + (t - t_g)\,\vec{v}(t_g)$ $+ \sum_{i=1}^{3}(t - t_i)\,\Delta V_i\,\mathrm{U}(t - t_i)\,\mathrm{U}(t_g - t_i)$ $\vec{v}(t) = \vec{v}(t_g) + \sum_{i=1}^{3}\,\Delta V_i\,\mathrm{U}(t - t_i)\,\mathrm{U}(t_g - t_i)$

in Figure 2.2. From geometry, θ' and ϕ', are equivalent to the target-centered angles θ and ϕ, also indicated in Figure 2.2. To be consistent with the formulation of the state equations in the target-centered frame, the angles θ and ϕ will be taken as the measured angles.

These angles are related to the position of the interceptor through the relation

$$y_{true} = h(x) \tag{2.10}$$

where

$$x \equiv [r_x\ r_y\ r_z\ v_x\ v_y\ v_z]^T \tag{2.11}$$

$$y_{true} \equiv \left[\ \theta_{true}\quad \phi_{true}\ \right]^T \tag{2.12}$$

$$h(x) \equiv \left[\ \tan^{-1}\frac{r_x}{r_y}\quad \tan^{-1}\frac{r_x}{\left[r_x^2 + r_y^2\right]^{1/2}}\ \right]^T \tag{2.13}$$

This expression allows computation of the true angles, θ_{true} and ϕ_{true}, from the true position. These angles will exactly match the measured values of θ and ϕ if there is no noise in the angle measurements. However, because the angle measurements are

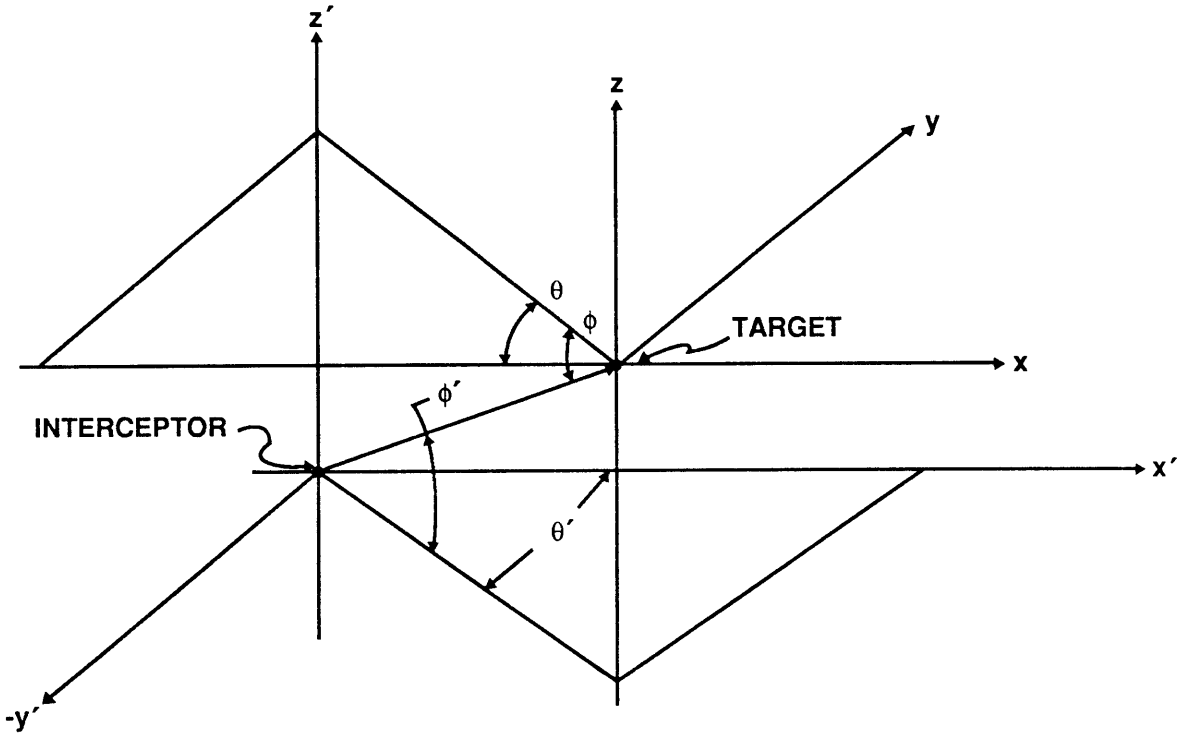

Figure 2.2. Interceptor Measurement Angles

corrupted by noise, the angles measured will differ from the true values. Modeling the noise as a Gaussian, white noise process gives

$$y = y_{true} + w = h(x) + w \tag{2.14}$$

where

$$\begin{aligned} y &\equiv \left[\begin{array}{cc} \theta & \phi \end{array} \right]^T_{measured} \\ w &\equiv \left[\begin{array}{cc} w_\theta & w_\phi \end{array} \right]^T \end{aligned}$$

Now, θ and ϕ represent the value of the angles measured by the interceptor. The variables w_θ and w_ϕ represent zero mean, Gaussian random numbers.

2.2 Guidance Model of the Navigation Filter

In order for the guidance to predict navigation filter performance, a model of the filter must be incorporated into the guidance algorithm. In this study, a continuous extended Kalman filter was used to predict the performance of the navigation filter (a discrete Kalman filter). The following sections review the Kalman filter equations and describe how they must be modified for use in the guidance algorithm.

2.2.1 Continuous Kalman Filter Equations

To develop the extended Kalman filter equations, the approach of Ref [4] was taken. This approach calls for the realization that the Kalman filter is actually an observer and allows the filter state and measurement estimate to be expressed in the form

$$\dot{\hat{x}} = A\hat{x} + u + K(y - \hat{y}) \tag{2.15}$$

$$\hat{y} = h(\hat{x}) \tag{2.16}$$

where

$$K = \text{extended Kalman gain matrix}$$

The most noticeable difference between the actual state given by equation 2.6 and the state estimate here is the additional term $K(y - \hat{y})$. The term, $(y - \hat{y})$, is called the *residual* and represents the difference between the actual measurement, y, and the estimated measurement, $\hat{y}$. It is this residual that allows the angle measurements to affect the state estimate (hopefully bringing the state estimate closer to the true state).

To complete the development of the extended Kalman filter requires that the state estimate given by equation 2.15 be linearized. This involves a Taylor series expansion of the residual about the filter state, $\hat{x}$. Subtracting equation 2.16 from equation 2.14 produces

$$y - \hat{y} = h(x) + w - h(\hat{x}) \tag{2.17}$$

But, a Taylor series expansion of $h(x)$ gives

$$h(x) = h(\hat{x}) + \left.\frac{\partial h}{\partial x}\right|_{\hat{x}} (x - \hat{x}) + \cdots \tag{2.18}$$

so that the residual can be approximated as

$$y - \hat{y} \approx \frac{\partial h(\hat{x})}{\partial x}(x - \hat{x}) + w \tag{2.19}$$

With these linearizations it is possible to compute the extended Kalman gain matrix. Continuing to follow the approach of Ref [4] produces the gain matrix

$$K = P\,C\,W^{-1} \tag{2.20}$$

where

$$P = \text{covariance matrix} \equiv \mathrm{E}\{(x-\hat{x})(x-\hat{x})^T\} \tag{2.21}$$

$$C \equiv \frac{\partial h(\hat{x})}{\partial x} \tag{2.22}$$

$$W \equiv \mathrm{E}\{w\,w^T\} \tag{2.23}$$

The matrix, W, represents the covariance matrix of the angle measurements and is an indicator of angle measurement quality. The matrix, P, represents the covariance matrix of the error in the state, where error is defined as the difference of the actual state from the estimated state. The value of the covariance matrix is obtained by integration of the matrix Ricatti equation

$$\dot{P} = A\,P + P\,A^T - P\,C^T\,W^{-1}\,C\,P \tag{2.24}$$

The first and second term on the right side of equation 2.24 produce changes in the covariance matrix simply from the dynamic behavior of the system. That is, if no measurements were taken, only these first two terms would be present. The third term results from the inclusion of the measurements and serves to decrease the uncertainty in the state estimate.

The equations of the continuous Kalman filter are summarized in Table 2.3. Further information on observers and Kalman filters can be found in References [4] and [5].

Table 2.3. Extended Kalman Filter Equations for Navigation

State Estimate	$\dot{\hat{x}} = A\hat{x} + u + K(y - \hat{y})$
Measurement Equation	$\hat{y} = h(\hat{x})$
Covariance Matrix	$\dot{P} = AP + PA^T - PC^TW^{-1}CP$

2.2.2 Kalman Filter Equations in the Guidance

In order for the guidance algorithm to use the Kalman filter equations of the previous section, the filter equations must be modified slightly. That is, the guidance algorithm can not simply integrate the equations of Table 2.3 to predict the covariance and state at some future time since these equations require the angle measurements, y. The measurements, y, have not been made beyond the current time. In order to propagate the state estimate, it is necessary to drop the residual term from the differential equation defining the state estimate. However, it is still necessary to predict the impact of future measurements on the covariance matrix. Thus, the matrix Ricatti equation defining covariance behavior remains unchanged.

The equations used by the guidance to predict filter performance are summarized in Table 2.4 and should be compared to those of Table 2.3

Notice that the modification converts the equation for the navigation filter state estimate into the same state equation of Section 2.1.1. This expression can be integrated to give the state estimate as a function of time, as given in Table 2.2.

Table 2.4. Extended Kalman Filter Equations for Guidance Prediction

State Estimate	$\dot{\hat{x}} = A\hat{x} + u$
Measurement Equation	$\hat{y} = h(\hat{x})$
Covariance Matrix	$\dot{P} = AP + PA^T - PC^TW^{-1}CP$

2.3 Variance in Time-to-go

To obtain an expression for the variance in time-to-go, an expression for time-to-go itself is required. In this study, time-to-go was defined to be time to the point of closest approach to the target. (It is at this point that the contact expander must be fully deployed.) To determine the time to closest approach, consider the target-interceptor geometry depicted in Figure 2.3. The point of closest approach is defined

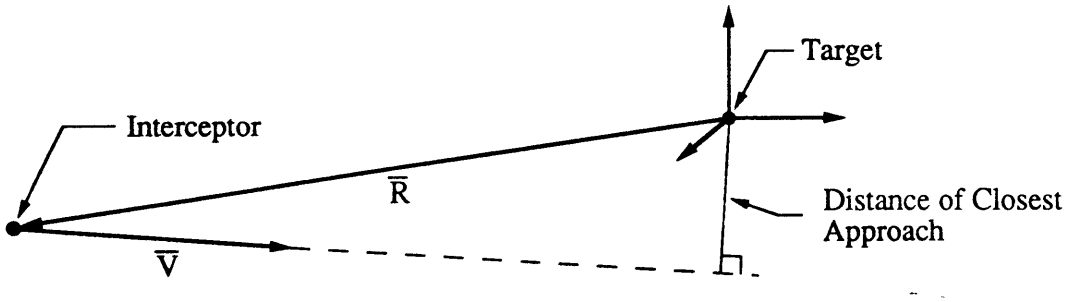

Figure 2.3. Target-Interceptor Geometry for Time-to-go Computation

as the shortest distance from the target to the path of the interceptor. The interceptor path is taken to be the projection of the current velocity vector. The distance the

interceptor must travel to reach this point, assuming no forces act on the interceptor, is given by

$$\frac{\vec{r} \cdot \vec{v}}{v}$$

The velocity at which the interceptor will traverse this distance is simply, v, giving a time-to-go of

$$t_{go} = \frac{\text{distance}}{\text{velocity}} = \frac{\vec{r} \cdot \vec{v}}{\vec{v} \cdot \vec{v}} \tag{2.25}$$

Now, using the definition of variance produces

$$\sigma^2_{tgo} \equiv \mathrm{E}\{(t_{go} - \bar{t}_{go})((t_{go} - \bar{t}_{go})^T\} \tag{2.26}$$

where

$$\bar{t}_{go} \quad = \quad \text{mean value of } t_{go} \equiv \mathrm{E}\{t_{go}\}$$

Because of the nonlinear relationship between t_{go}, $\vec{r}$, and $\vec{v}$ in equation 2.25, the exact value of $\bar{t}_{go}$ would be difficult to compute. As an approximation, $t_{go}(\hat{x})$ is used. This approximation, as well as the first order Taylor series expansion of time-to-go about the estimated state

$$t_{go} \approx t_{go}(\hat{x}) + \left.\frac{\partial t_{go}}{\partial x}\right|_{\hat{x}} (x - \hat{x}) \tag{2.27}$$

allows the variance in time-to-go to be written in the form

$$\sigma^2_{tgo} \approx \mathrm{E}\{m^T(x - \hat{x})(x - \hat{x})^T m\} \tag{2.28}$$

where

$$m^T \equiv \left.\frac{\partial t_{go}}{\partial x}\right|_{\hat{x}}$$

Since m is not a random variable, it can be brought outside the expectation operator to give

$$\sigma_{tgo}^2 = m^T P m \tag{2.29}$$

This expression relates variance in time-to-go to the state covariance defined by equation 2.21.

2.4 Fuel Usage

The remaining term in the cost function to be described is fuel usage. Fuel usage is included in the cost function as the square of the magnitude of all velocity changes. Notationally, fuel usage is broken into two terms, one for estimation enhancement maneuvers, ΔV, and one for intercept, $\Delta V_{hit} = \Delta V_3$. Note that ΔV is a six element vector containing both ΔV_1 and ΔV_2. It is these two maneuvers that the guidance is free to select when minimizing the cost function. The final hit maneuver, ΔV_{hit}, is not an independent variable to be used in the minimization process since it must be selected to provide intercept at the desired time. This is fixed by the physics of the situation. However, the term is still included in the cost function because it represents fuel usage.

To determine ΔV_{hit}, the equations of Table 2.2 can be used. Setting the position at the final time, t_f, to $\vec{0}$, gives

$$\vec{r}(t_f) = \vec{0} = r(t_g) + (t_f - t_g)\,\vec{v}(t_g) + \sum_{i=1}^{3}(t_f - t_i)\,\Delta V_i\,\mathrm{U}(t_g - t_i) \tag{2.30}$$

Solving for ΔV_{hit} gives

$$\Delta V_{hit} \equiv \Delta V_3 = \frac{-1}{(t_f - t_3)} \left[\vec{r}(t_g) + (t_f - t_g)\vec{v}(t_g) + \sum_{i=1}^{2} (t_f - t_i)\, \Delta V_i\, \mathrm{U}(t_g - t_i) \right] \tag{2.31}$$

Notice that the term in the bracket represents the position of the interceptor at the final time, t_f, if no final hit maneuver is performed. Letting $\vec{r}_{nh}(t_f)$ denote this position allows ΔV_{hit} to be written compactly as

$$\Delta V_{hit} = \frac{-1}{(t_f - t_3)} \vec{r}_{nh}(t_f) \tag{2.32}$$

where

$$\vec{r}_{nh}(t_f) = \left[\vec{r}(t_g) + (t_f - t_g)\vec{v}(t_g) + \sum_{i=1}^{2} (t_f - t_i)\, \Delta V_i\, \mathrm{U}(t_g - t_i) \right] \tag{2.33}$$

2.5 Total Cost Function

Combining each element of Section 2.3 and 2.4 produces the final expression for the cost function

$$J = \frac{1}{2} \Delta V^T \Delta V + \frac{1}{2} \Delta V_{hit}^T \Delta V_{hit} + f\, \sigma_{tgo}^2 \Big|_{t=t_3} \tag{2.34}$$

where:

$$\begin{aligned} f &= \text{weight factor for variance in time-to-go} \\ \Delta V^T &= [\Delta V_1^T\ \Delta V_2^T] \\ \sigma_{tgo}^2(t) &= m^T(\hat{x}(t))\, P(t, \hat{x}(t))\, m(\hat{x}(t)) \end{aligned} \tag{2.35}$$

Equation 2.34 represents the cost function that the guidance must minimize before each maneuver.

In computing the cost, J, for a given ΔV, it is evident from equation 2.34 that the guidance must predict both ΔV_{hit} and σ^2_{tgo}. The prediction for ΔV_{hit} is a straight forward application of equation 2.32. The prediction of σ^2_{tgo} requires the covariance matrix and state estimate at the time, t_3, as evident from equation 2.35. This is obtained by integration of the differential equations of Table 2.4.

Chapter 3

Cost Function Minimization

With the cost function defined, the problem now becomes one of minimization—find the maneuvers, ΔV_1 and ΔV_2, that minimize J. In Ref [6], Strang presents several different techniques for performing a function minimization—steepest descent, conjugate gradient, Newton's Method, etc. From the author's experience minimizing this particular cost function, it has been observed that J suffers from the classic "long, narrow valley" condition described in Ref [6]. That is, if J were plotted as a function of the independent variables (ΔV_1 and ΔV_2), the surface of J would look similar to that depicted in Figure 3.1. This condition virtually eliminates the use of steepest descent in finding the minimum. (At least if the minimum is to be found quickly.) The actual minimization procedure developed for this study is similar to the conjugate gradient search algorithm. The algorithm requires an expression for

$$\frac{\partial J}{\partial \Delta V}$$

This chapter presents the expressions necessary to compute the partial of J with respect to ΔV. It also further describes the search algorithm used to minimize J.

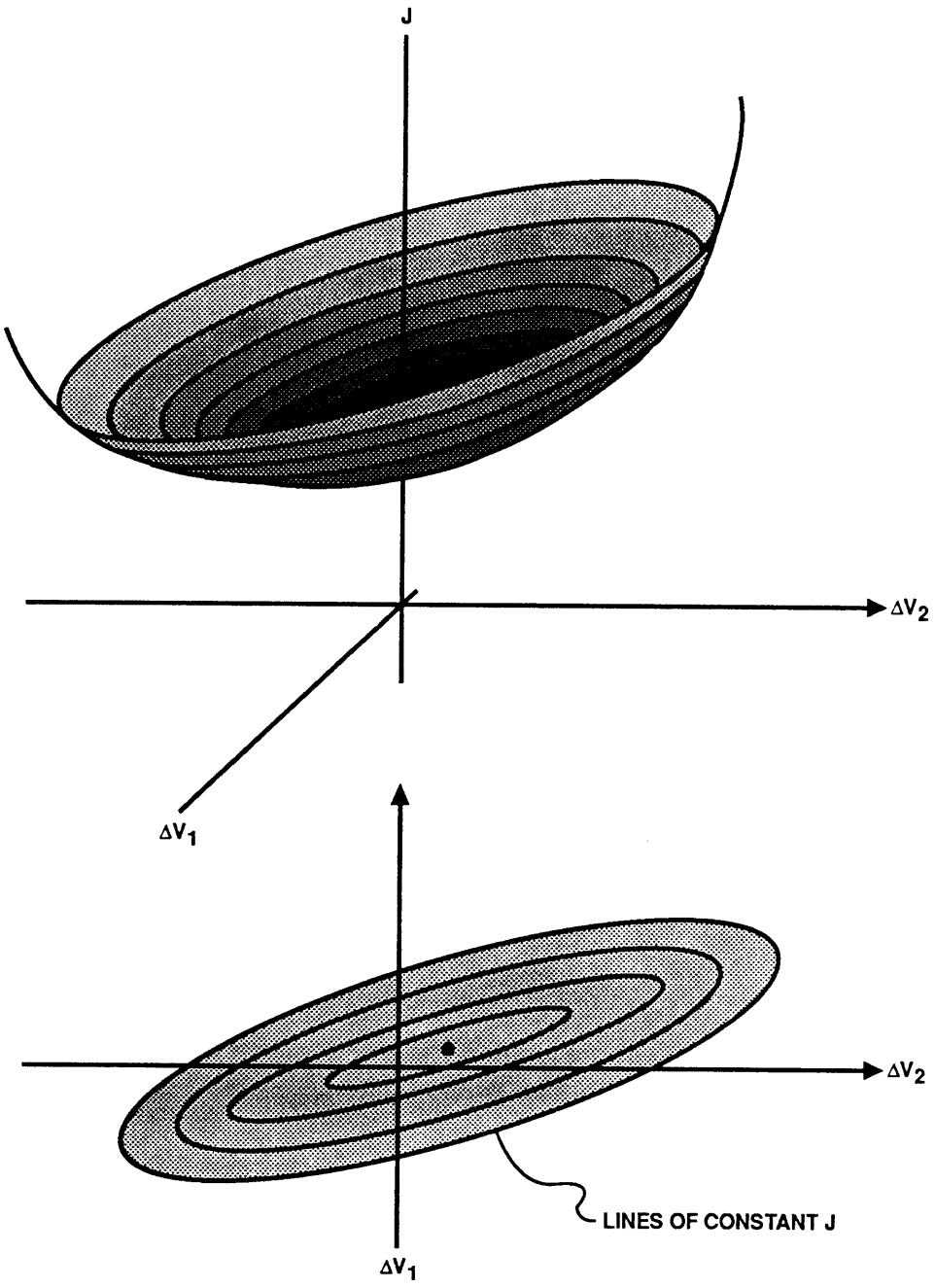

Figure 3.1. Classic "Long, Narrow Valley" Condition

3.1 Cost Function Gradient

To begin the computation of the partial of J with respect to ΔV, the cost function has been rewritten below.

$$J = \frac{1}{2}\Delta V^T \Delta V + \frac{1}{2}\Delta V_{hit}^T \Delta V_{hit} + f\,\sigma_{tgo}^2\Big|_{t=t_3} \tag{3.1}$$

Taking the partial of J with respect to ΔV gives

$$\frac{\partial J}{\partial \Delta V} = \Delta V^T + \Delta V_{hit}^T \frac{\partial \Delta V_{hit}}{\partial \Delta V} + f\,\frac{\partial \sigma_{tgo}^2}{\partial \Delta V}\Big|_{t=t_3} \tag{3.2}$$

The middle term involving the partial of ΔV_{hit} can be expanded using the expression for ΔV_{hit} from Section 2.4. Using equation 2.32 produces

$$\frac{\partial \Delta V_{hit}}{\partial \Delta V} = \frac{-1}{(t_f - t_3)}\frac{\partial \vec{r}_{nh}(t_f)}{\partial \Delta V} \tag{3.3}$$

The term, $\vec{r}_{nh}(t_f)$, indicates the predicted position of the interceptor at the scheduled intercept time when no final hit maneuver is performed. An expression for the partial of $\vec{r}_{nh}(t_f)$ is obtained by differentiation of equation 2.33.

The last term of equation 3.2, involving σ_{tgo}^2, can be expanded using the expression for the variance from Section 2.3. Using equation 2.29 gives

$$\frac{\partial \sigma_{tgo}^2}{\partial \Delta V} = 2m^T P \frac{\partial m}{\partial \Delta V} + m^T \frac{\partial P}{\partial \Delta V} m \tag{3.4}$$

Application of the chain rule in determining equation 3.4 generates two partials, one involving the time-to-go measurement sensitivity vector, m, and the other involving the covariance matrix, P. Computation of the partial of m with respect to ΔV is

straightforward and again involves the use of the chain rule, which allows the partial to be written as

$$\frac{\partial m}{\partial \Delta V} = \frac{\partial m}{\partial \hat{x}} \frac{\partial \hat{x}}{\partial \Delta V} \tag{3.5}$$

with

$$m = \left[-\frac{\vec{v}^T}{v^2} \quad -\frac{\vec{r}^T}{v^2} + 2\frac{(\vec{r}\cdot\vec{v})}{v^4} v^T \right] \tag{3.6}$$

$$\frac{\partial m}{\partial \hat{x}} = \begin{bmatrix} 0 & -\frac{1}{v^2} I + \frac{2}{v^4}\vec{v}\vec{v}^T \\ -\frac{1}{v^2} I + \frac{2}{v^4}\vec{v}\vec{v}^T & 2\frac{(\vec{r}\cdot\vec{v})}{v^6}\left[v^2 I - 4\vec{v}\vec{v}^T\right] \end{bmatrix} \tag{3.7}$$

An expression for the partial of $\hat{x}$ in equation 3.5 can be found by differentiating the state equations of Table 2.2.

The final term, for which no expression has yet been given, is the last term of equation 3.4—namely, the partial of P with respect to ΔV. This term involves, by far, the largest computational effort. The derivation of an analytic expression for this term starts with the matrix identity

$$\frac{dA(x)}{dx} = -A(x)\frac{dA^{-1}(x)}{dx}A(x)$$

This identity permits the partial of P with respect to ΔV to be written in terms of the inverse of the covariance matrix, or information matrix, S, as

$$\left.\frac{\partial P}{\partial \Delta V}\right|_{t=t_3} = -\left[P \frac{\partial S}{\partial \Delta V} P \right]_{t=t_3} \tag{3.8}$$

From section 2.2.2, $P(t_3)$ can be found by integrating the matrix Ricatti equation

$$\dot{P} = A\,P + P\,A^T - P\,C^T\,W^{-1}\,C\,P \tag{3.9}$$

Equations 3.8 and 3.9 convert the problem of finding the partial of P with respect to ΔV into one of finding the partial of S with respect to ΔV. This computation is facilitated by the use of the matrix identity

$$\frac{dA^{-1}}{dx} = -A^{-1}(x)\frac{dA(x)}{dx}A^{-1}(x)$$

which allows conversion of the matrix Ricatti equation, involving the covariance matrix, into a differential equation involving the information matrix. Pre- and post-multiplying equation 3.9 by P^{-1} produces the desired matrix differential equation

$$\dot{S} = -SA - A^T S + C^T W^{-1} C \tag{3.10}$$

This expression can be integrated to give

$$S(t) = \Phi^{-T}(t,t_s)S(t_s)\Phi^{-1}(t,t_s) + \int_{t_s}^{t} \Phi^{-T}(t,\lambda)C^T(\lambda)W^{-1}(\lambda)C(\lambda)\Phi^{-1}(t,\lambda)d\lambda \tag{3.11}$$

where the state transition matrix, $\Phi(t,t_s)$, is the solution of the homogeneous system

$$\dot{\hat{x}} = A\hat{x} \implies \Phi(t,t_s) = e^{A(t-t_s)} \tag{3.12}$$

It is equation 3.11 that allows computation of the partial of S with respect to ΔV. Fortunately, the state transition matrix, Φ, is not a function of ΔV. This allows the partial of S to be written in the form

$$\frac{\partial S}{\partial \Delta V} = \int_{t_s}^{t} \Phi^{-T}(t,\lambda)\frac{\partial H(\lambda)}{\partial \Delta V}\Phi^{-1}(t,\lambda)d\lambda \tag{3.13}$$

where

$$H(\lambda) \equiv C^T(\lambda)W^{-1}(\lambda)C(\lambda)$$

Using the chain rule to compute the partial of H with respect to ΔV gives

$$\frac{\partial H}{\partial \Delta V} = \frac{\partial C^T}{\partial \Delta V} W^{-1} C + C^T W^{-1} \frac{\partial C}{\partial \Delta V} \tag{3.14}$$

which can also be written as

$$\frac{\partial H}{\partial \Delta V} = \left[C^T W^{-T} \frac{\partial C}{\partial \Delta V} \right]^T + C^T W^{-1} \frac{\partial C}{\partial \Delta V} \tag{3.15}$$

Analytically, there is no difference between equation 3.14 and equation 3.15, but equation 3.15 eliminates any deceptive need for two partials. In equation 3.14, it appears that the partial of both C and C^T are needed. In equation 3.15, it is clear that only the partial of C is needed. The desired partial of C can be found using the chain rule to give

$$\frac{\partial C}{\partial \Delta V} = \frac{\partial C}{\partial \hat{x}} \frac{\partial \hat{x}}{\partial \Delta V} \tag{3.16}$$

An expression for the tensor, $\frac{\partial C}{\partial \hat{x}}$, can be found by differentiation of equation 2.22 in the previous chapter.

3.2 Minimization Algorithm

Minimization of the cost function is performed using an algorithm similar to conjugate gradient. Because the surface defined by J has a long, narrow valley, the following technique can be utilized. The procedure, as presented below, has not been optimized for implementation. Rather, it is presented in a manner that facilitates explanation.

The overall scheme is as follows. Suppose that the contours in Figure 3.2 represent lines of constant J. Minimization of J along the line, L, whose direction has been

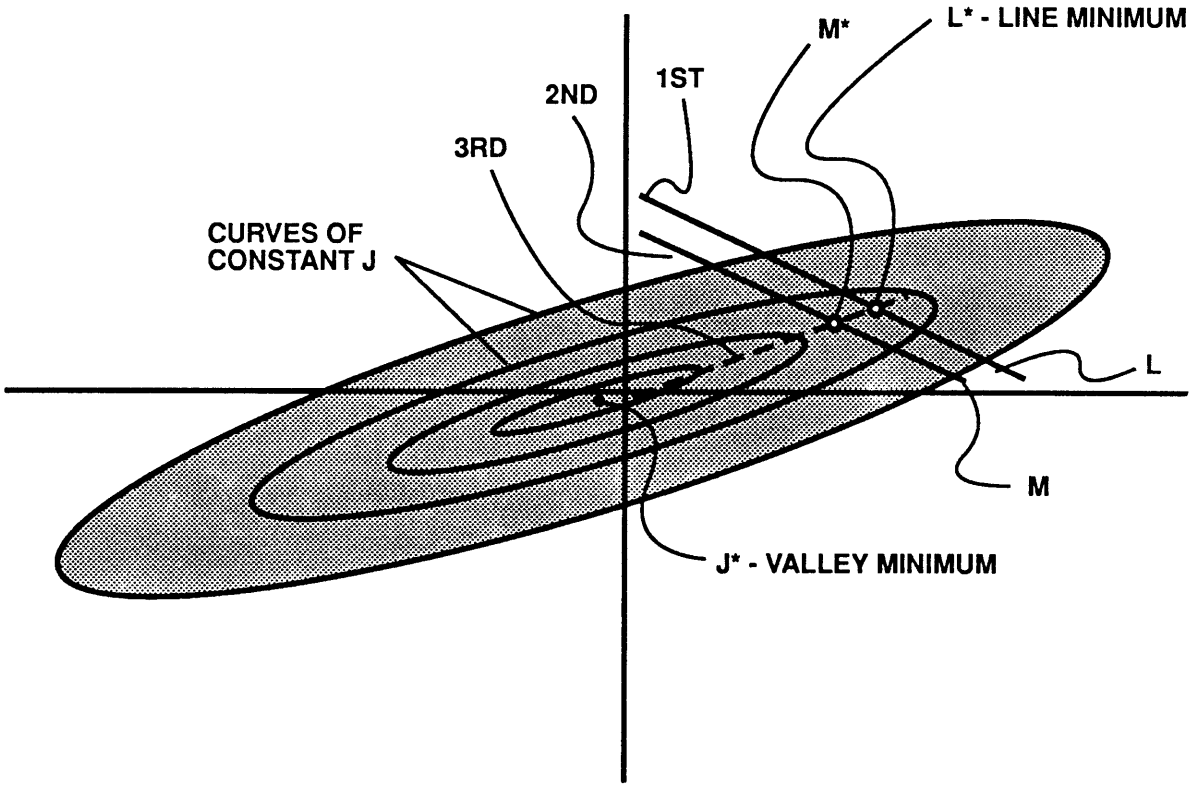

Figure 3.2. Curves of Constant J.

chosen arbitrarily, results in a minimum at the point L^*. Minimization along a second line, M, parallel to L but passing through a point displaced from L^*, results in a minimum at the point M^*. Now, the line connecting L^* and M^* points in the general direction of the valley minimum, J^*. Minimization in this new direction produces a minimum much closer to J^* than either L^* or M^*. Repeated application of this minimization technique will reveal the valley minimum, J^*.

Implementation of this algorithm first requires the selection of an arbitrary direction, $\hat{l}$ (assumed to be a unit vector), and an arbitrary point l. The algorithm starts by minimizing J along the line defined by the point, l, and the direction, $\hat{l}$.

To perform minimization along the line, the algorithm attempts to bracket the minimum along the line and then perform interval bisection. The bracketing search starts from the point l, where the partial of J with respect to ΔV is computed. Performing the dot product

$$\left.\frac{\partial J}{\partial \Delta V}\right|_l \cdot \hat{l}$$

produces the slope of J in the direction of $\hat{l}$. If the slope is negative, the point l becomes the left limit for interval bisection. If the slope is positive, the point l becomes the right limit. This can be verified by considering the cross-section of J along L depicted in Figure 3.3. In this figure, the slope of J in the direction of $\hat{l}$ is negative so the point, l, becomes the left limit.

With one of the bracket limits determined, it becomes necessary to determine the other limit. This is performed by moving along L in the *proper* direction until the dot product changes sign. The *proper* direction depends on which bracket limit has

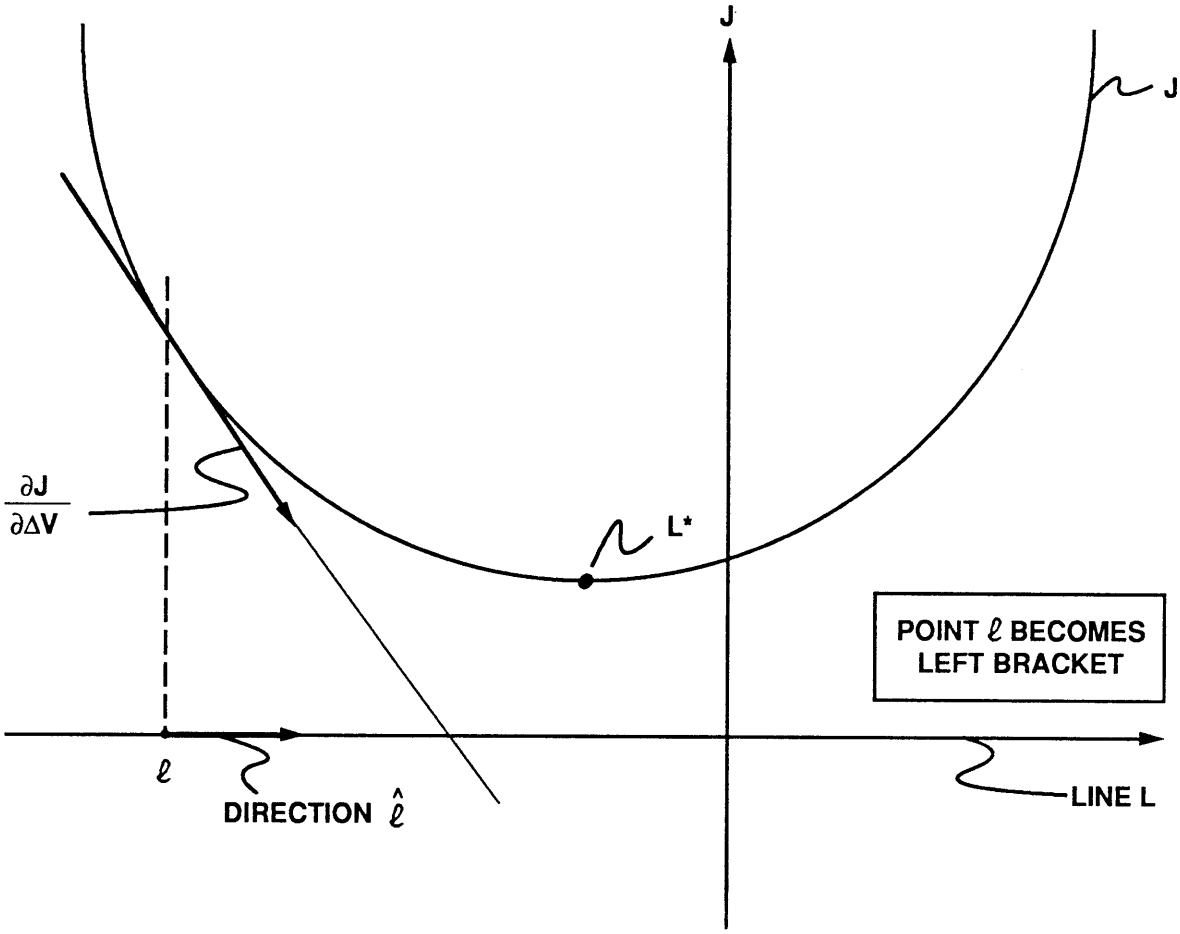

Figure 3.3. Cross Section of J along line L.

already been found. If the left limit (defined by a negative dot product) has been found, it is necessary to move in the direction of $\hat{l}$. If the right limit has been found, it is necessary to move in the opposite direction of $\hat{l}$.

With the *proper* direction determined, it is necessary to select an arbitrary distance, d, by which to move along L from the current point l. The distance should be large enough so that the other bracket limit can be found quickly. It is better to spend only a few iterations finding the other bracket limit, and then perform interval bisection, than to spend many iterations, taking small steps, in search of the other bracket limit. The actual distance, d, used in this guidance study was selected heuristically based on several trial minimizations.

After moving along L a sufficient number of steps to a point, m, the dot product

$$\left.\frac{\partial J}{\partial \Delta V}\right|_m \cdot \hat{l}$$

should change sign, indicating the other bracket limit has been found. The points, l and m, define the limits between which an interval bisection search is performed. Performing bisection until the slope of J in the direction of $\hat{l}$ reaches some tolerance, produces the minimum, L^*, along the line L. This point, L^*, will be saved to determine a new search direction. However, another line minimization must be performed before a new search direction can be found.

A new line, K, offset from L, is defined by a point displaced from the previous line minimum, L^*, and the same direction, $\hat{l}$. (In the actual guidance implementation, the amount the new point was displaced from the line minimum, L^*, was selected heuristically based on several trail minimizations.) Performing the same search algorithm

on this line results in a line minimum at the point, K^*. The line connecting the two minimum, L^* and K^*, defines a new search direction that points in the general direction of the valley minimum, J^*. This dual line minimization process is started anew with the new search direction just determined. The starting point on this new line should be either K^* or L^*, depending on which is closer to J^*. This can be determined from the slope of J in the new direction. The entire search is performed until

$$\left| \frac{\partial J}{\partial \Delta V} \right|$$

falls below some tolerance value.

Chapter 4

Guidance Implementation and Simulation

In order to evaluate the performance of the guidance algorithm, a computer simulation of the intercept was developed. This chapter describes the implementation of the simulation, including the guidance algorithm, and reviews the assumptions made during its development. To that end, the following sections sequentially review the major simulation components listed in Table 4.1. (Figure 4.1 depicts the interaction between each of the components.) The first element of Table 4.1, the Executive routine, controls overall simulation sequencing and initialization, as well as data I/O. Its essential function is to perform calls to the other elements of the simulation and maintain a rigorous separation between true and estimated states. It will not be discussed further.

Section 4.1 begins with a description of the Environment routine and the model it uses to define the true state of each vehicle. Section 4.2 then describes the interceptor's navigation filter and the rate at which navigation filter updates occur.

Table 4.1. Major Components of Computer Simulation

Program Component	Purpose
Executive	Main routine that handles handshaking between and calling of major simulation components.
Environment	Maintains the "true" state of the interceptor and target.
Navigation	Maintains the estimated states of the target using discrete Kalman filtering of the angle measurements.
Guidance	Determines the maneuvers that minimize the cost function.

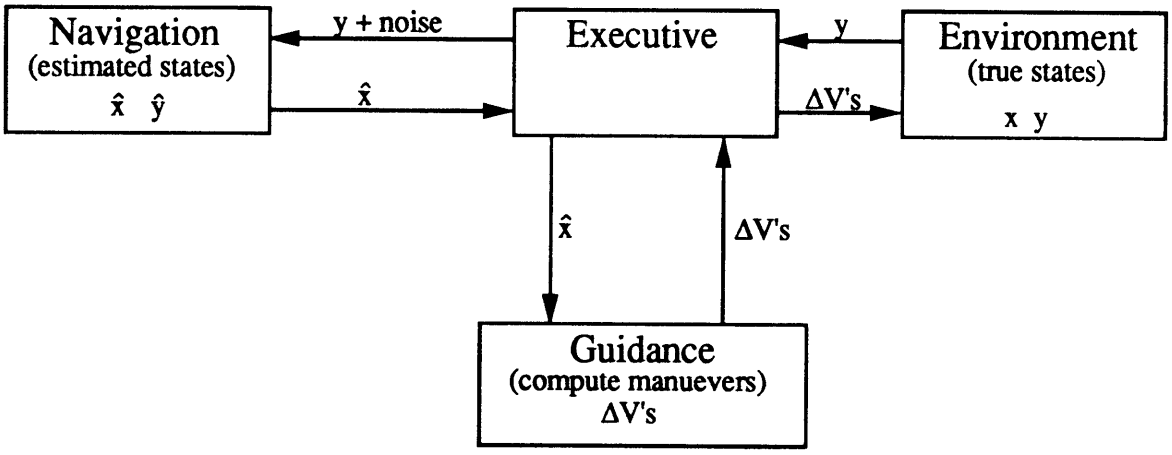

Figure 4.1. Interaction Between Simulation Components

Section 4.3 reviews implementation of the guidance and addresses the computation of ΔV_{hit}. (The theory of the previous chapters concerns only the selection of ΔV_1 and ΔV_2, not ΔV_{hit}.) Finally, in Section 4.4, the procedure used to determine initial conditions for the various intercept scenario's is reviewed. This procedure allows the performance of the guidance algorithm to be examined for different target-interceptor closing geometries.

4.1 Environment Routine

To perform the simulation, it is necessary to have a routine that determines the true state of both the interceptor and target throughout the simulated mission. This function is performed by the Environment routine. In the Environment routine, each vehicle is modeled as a point mass under the influence of a gravitational field. This is justified by considering the altitude at which the entire mission takes place. At 200km above the surface of the earth, the most significant force acting on a body is gravity. Particle drag, $J2$ effects, etc. will not significantly affect the motion of the vehicles. The equations of motion for the point masses in this gravitational field become

$$\ddot{\vec{r}}_{i_{EF}} = -\frac{\mu}{(r_{i_{EF}})^3}\vec{r}_{i_{EF}} \quad \text{and} \quad \ddot{\vec{r}}_{t_{EF}} = -\frac{\mu}{(r_{t_{EF}})^3}\vec{r}_{t_{EF}} \tag{4.1}$$

where

$$\mu = 1.4076468532 \times 10^{16}\ \text{ft}^3/\text{sec}^2$$

represents the gravitational parameter and, $r_{i_{EF}}$ and $r_{t_{EF}}$, the distances from the center of the planet to the interceptor and target, respectively. The subscript 'EF'

indicates coordinatization in an earth fixed frame. As the simulation proceeds, the Environment routine integrates Equations 4.1 using a fourth order Runga-Kutta algorithm. Further information concerning the equations of motion for a body in a central force field can be found in Ref [7].

4.2 Navigation Routine

In order for the guidance algorithm to function, the interceptor must know its state relative to the target. Because of initial condition errors in the position and velocity estimate of the target, the interceptor will not know its true state relative to the target and must, therefore, form an estimated state. In this study, the estimated state is obtained using an "optimal" estimator—a discrete extended Kalman filter—and is implemented within the navigation routine.

The Kalman filter performs three tasks during the estimation process. First, it takes the current state estimate and angle measurements and determines an improved state estimate. Second, it propagates the estimated state forward between measurements. Finally, the Kalman filter provides a measure of it's own performance by maintaining a covariance matrix which indicates the accuracy of the estimated state.

Implementation of the navigation filter is based on the continuous-discrete extended Kalman filter equations presented in Ref [5]. The continuous portion of the Kalman filter formulation refers to the system model used to predict interceptor motion. This is written in the form

$$\dot{x}(t) = f(x(t), t)$$

and is a continuous expression in time. The system model used within the navigation filter is identical to the equations of motion used in the environment routine. The equations can be found in Section 4.1

The discrete portion of the Kalman filter formulation refers to the measurement model used to predict angle measurements when they are taken. Since the angle measurements occur at discrete times, the measurement model can be written in the form

$$y_k = h_k(x(t_k)) + w_k$$

where w_k is a white sequence of zero mean gaussian random numbers representing the noise in the angle measurements. The term, $h_k(x(t_k))$, allows computation of the measurements (θ and ϕ) from the current state and is identical to $h(x)$ in Equation 2.13.

With the system and measurement model described, it is now possible to summarize the equations used to propagate and update the state estimate and covariance matrix. Table 4.2 contains the necessary equations.

Since the discrete Kalman filter must process measurements at specific points in time, a brief comment is appropriate concerning the rate at which the filter processes measurements. The frequency of filter update is depicted in Figure 4.2. As evident from the figure, the filter processes angle measurements at a rate of 1 per second, except for the regions close to the burns, where no measurements are taken. The modeling decision to place a 5 second "dead time" before and after each burn allows a realistic amount of time for the burn to occur—even though the burn is still applied

Table 4.2. Continuous-Discrete Extended Kalman Filter Equations

State Estimate Propagation	$\dot{\hat{x}}(t) = f(x(t), t)$
State Covariance Propagation	$\dot{P}(t) = F(\hat{x}(t), t)\, P + P\, F^T(\hat{x}(t), t)$
State Estimate Update	$\hat{x}_k^+ = \hat{x}_k^- + K_k \left[y_k - h_k(\hat{x}_k^-) \right]$
State Covariance Update	$P_k^+ = \left[\mathrm{I} - K_k\, H_k(\hat{x}_k^-) \right] P_k^-$
Kalman Gain Matrix	$K_k = P_k^-\, H_k^T(\hat{x}_k^-) \left[H_k(\hat{x}_k^-)\, P_k^-\, H_k^T(\hat{x}_k^-) + R_k \right]^{-1}$
where	$R_k \equiv \mathrm{E}\{w_k w_k^T\}$ $F(\hat{x}(t), t) \equiv \left. \dfrac{\partial f(x(t), t)}{\partial x(t)} \right\|_{x(t)=\hat{x}(t)}$ $H_k(\hat{x}_k^-) \equiv \left. \dfrac{\partial h_k(x(t_k))}{\partial x(t_k)} \right\|_{x(t_k)=\hat{x}_k^-}$

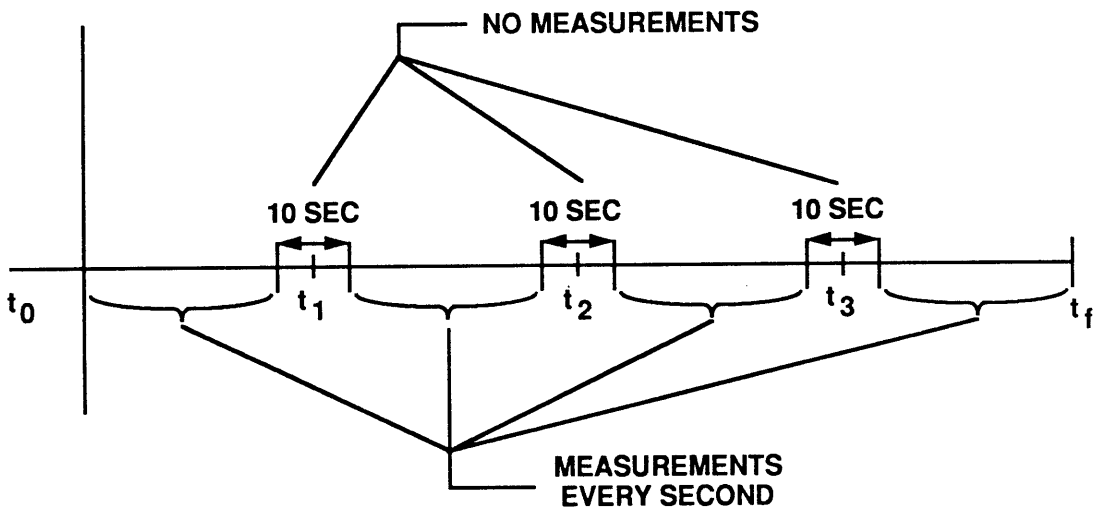

Figure 4.2. Timeline of Navigation Filter Updates

impulsively within the simulation. The dead time would result because angle measurements can not be made when the interceptor is thrusting. The addition of this dead time to the simulation means that the guidance will predict a slightly smaller variance in t_{go} at $t = t_3$ than the actual variance. This is because the guidance model was developed under the assumption that angle measurements would be uninterrupted from t_0 to t_3. However, the difference between the actual variance and that predicted by the guidance will be small because the dead time period is relatively short when compared to the overall mission time.

4.3 Guidance Routine

This section considers two factors that affect guidance implementation that are not addressed in Chapters 2 and 3. The first concerns the choice of directions for the coordinate axes and it's effect on minimizing J. In the previous chapters, the equations necessary to determine ΔV_1 and ΔV_2 are derived for the general orientation of coordinate axes. If the coordinate axes are selected properly, two practical considerations allow a substantial reduction in the number of independent variables required to perform the minimization. Section 4.3.1 describes both the coordinate system and the practical considerations that allow this reduction.

The second factor to be addressed here is the computation of ΔV_{hit} when the interceptor reaches the point in the trajectory where ΔV_{hit} is to be applied. The previous chapters do not specify the actual computation of ΔV_{hit}. An approximation to ΔV_{hit} is used when determining the cost function minimizing velocity corrections,

ΔV_1 and ΔV_2. Section 4.3.2 describes the equations used to determine ΔV_{hit} when it is needed for intercept.

4.3.1 Reducing the Dimensionality of J

Before combining the equations of Chapters 2 and 3 into a guidance algorithm, a judicious selection of coordinate systems and a consideration for both time-to-go and problem symmetry permit a substantial reduction in the dimensionality of J. As developed, the cost function J depends on 6 independent variables—ΔV_1 and ΔV_2. It is possible to reduce the dimensionality of J such that J depends only on one component of ΔV_1 and one of ΔV_2. This reduction in dimensionality provides a worthwhile reduction in the computational effort required to minimize J.

Coordinate Systems

A reduction in the dimensionality of J begins with the inertial coordinate frame, XYZ, first introduced in Section 2.1.1. In that section, the equations of motion for the interceptor are developed in a target centered frame, xyz, whose coordinate axes are defined to be parallel to XYZ. Rather than first specifying the direction of the coordinate axes, XYZ, it is convenient to specify the direction of the coordinate axes, xyz, and then take the direction of the XYZ axes to be parallel to those of xyz.

Fortunately, at no point in the development of Section 2.1.1 was the direction of the coordinate axes XYZ, and thus xyz, specified. No loss of generality results by taking the direction of the x-axis to be along the line-of-sight from the target to the interceptor (ie. position vector from the target to the interceptor) at the time of the

guidance call. Thus, when the guidance algorithm begins it's prediction of σ^2_{tgo} and ΔV_{hit}, the position vector contains only one non-zero component, r_x.

With the direction of the x-axes determined, the direction of the z-axis can be uniquely specified as both

- orthogonal to the x-axis and
- contained in the plane determined by the position and velocity vectors of the interceptor relative to the target.

The final coordinate direction, y, must then be taken orthogonal to both x and z. The orientation of the xyz coordinate frame is depicted in Figure 4.3.

Consideration of Time-to-go

The first consideration that follows from this choice of coordinate directions concerns the effect of maneuvers on the time-to-go. If the interceptor is allowed to perform velocity changes in the line-of-sight direction, a change in time-to-go will occur. To prevent this, the guidance algorithm does not use ΔV_{1_x} and ΔV_{2_x} in the minimization process. That is, ΔV_{1_x} and ΔV_{2_x} are both set equal to 0. Thus, all maneuvers are restricted to be in the plane normal to the line-of-sight, hereafter referred to as the normal directions, y and z.

It is interesting to note that, without the above restriction, the nature of the cost function is to radically reduce the interceptors velocity in the line-of-sight direction and have it "circle" the target. This significantly changes the time-to-go but enhances

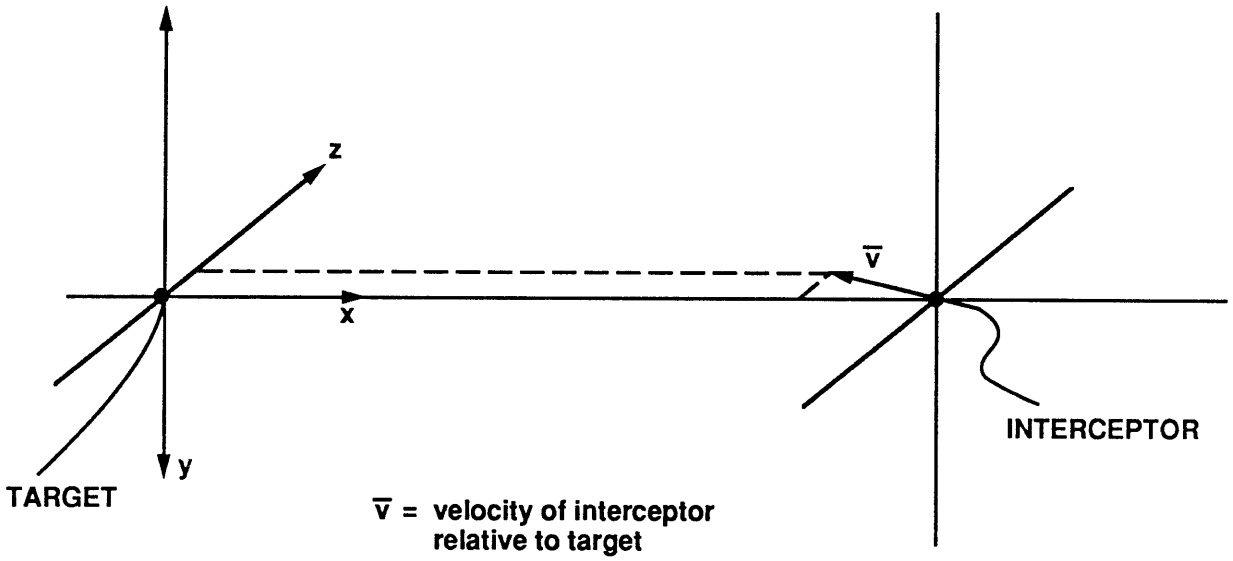

Figure 4.3. Orientation of the xyz Coordinate Frame

the observability of t_{go} because the interceptor gets an accurate measure of the targets position components. In a future analysis, it might prove interesting to release the constraint on maneuvers in the line-of-sight direction but to put a cost on a delayed t_{go}.

Consideration of Problem Symmetry

A further reduction in dimensionality follows from a consideration of the symmetry of the problem in the xyz coordinate system just described. To simplify the discussion, consider the special case defined by the following conditions at the time of a guidance call.

- The interceptor is heading straight for the target. It's position and velocity vectors each contain only one non-zero component, r_x and v_x, respectively.
- The state variances in the directions normal to the line-of-sight are equal.
- The quality of the angle measurements is not direction dependent.

After a few measurements the largest state variances will be in the line-of-sight direction. When the guidance attempts to minimize J by selecting the information-enhancing maneuvers, (ie. maneuvers that reduce the large variances in the line-of-sight direction) there will be no reason for the guidance to prefer maneuvers in the y direction over the z direction because of the axial symmetry about the line-of-sight direction.

Now, if the interceptor has an initial velocity with a component normal to the line-of-sight, it will perform maneuvers that utilize this normal component. That is, the guidance will apply an impulse that is in the same direction as this normal component to bring the interceptor to the furthermost point from the initial line-of-sight before the next maneuver. This allows the interceptor to maximize the angle between the initial line-of-sight and the line-of-sight before the next maneuver. This results in the largest observability and thus, the largest reduction in the state variances in the line-of-sight direction.

This consideration suggests that the relative motion can be constrained to a plane containing the normal velocity, if any, and that the guidance need only perform maneuvers in the direction of this initial normal velocity. Given the current selection of coordinate axes, this is in the direction of the z-axis. Thus, the second component of the velocity corrections that can be eliminated from the minimization process is the y component. This leaves minimization of J requiring the selection of ΔV_{1_z} and ΔV_{2_z} only.

It is worth pointing out that the minimization algorithm searched only for the minimum velocity corrections that were in the same direction as the normal component of the initial velocity. It is also true that the cost function has another minimum for velocity corrections that are applied in the opposite direction as the normal component of the initial velocity. These velocity corrections tend to have a slightly smaller ΔV_{hit}, but a slightly larger ΔV_1 and ΔV_2, than those obtained from a search where the velocity corrections are in the same direction as the normal component of initial

velocity. The actual difference in the value of the cost function for the two different minima is very small since the value of the initial normal velocity is small.

4.3.2 Computation of ΔV_{hit}

The Guidance routine computes all mid-course corrections (ΔV_1, ΔV_2, and ΔV_{hit}) that are to be applied along the trajectory. When the first two maneuvers, ΔV_1 and ΔV_2, are determined from the cost function minimization of Chapter 3, ΔV_{hit} is approximated using Equation 2.32. When the interceptor reaches the point in the trajectory where ΔV_{hit} must be applied, the guidance must compute ΔV_{hit}, to cause intercept with the target at the scheduled time. At this point in the trajectory it is no longer appropriate to use the approximation of Equation 2.32. Rather, a more accurate expression can be obtained using the orbital transfer equations of Ref [8]. Using the solution to Lambert's problem from this text allows ΔV_{hit} to be computed as a function of current position, target position at the scheduled time of intercept, and t_{go}.

4.4 Initial Conditions for the Simulation

In order to evaluate the performance of the guidance algorithm, various target-interceptor closing geometries were considered. All trajectories were developed under the assumption that the earth is spherical with no atmosphere. The development began by placing the target in a circular polar orbit at an altitude of 214 nm. Because the target was non-evasive, the point of intercept on this polar orbit was the same

nominal point for all trajectories.

Ten different trajectories were developed by placing the interceptor at various ranges (500 and 1000 nm) and bearing angles (0°, 45°, 90°, 135°, and 180°) from the ground projection of the intercept point. The 0° intercept is referred to as "head-on" and the 180° as "tail chase". Once the intercept point and target locations were selected, the interceptor was given the minimum impulsive boost required to reach the intercept point. Using this impulsive boost, the interceptor and target states were computed at the point of intercept. The states of both vehicles were then integrated backwards in time until the range between the two was 540 nm (1000 km). This distance is the maximum range of the angle sensor and is often called lock-on range. The states of both vehicles at this 540 nm range were used to initialize the simulation.

As a matter of interest the interceptor trajectories have higher apogees than the target. Thus, the interceptor is at a higher altitude than the target when lock-on occurs. The intercept altitudes at lock-on range vary from 260 nm to 292 nm.

As a further matter of interest the initial interceptor range of 1000 nm is the ground distance between two successive polar orbits at a latitude of 40°. Crudely speaking, there should be two or three successive launch opportunities for targeting a vehicle in such a polar orbit. On the first pass the target would be about 1000 nm to the east, on the next pass the target would pass directly overhead, and on the last pass the target would pass by about 1000 nm to the west.

Chapter 5

Performance Results

This chapter describes the performance and behavior of the guidance algorithm for the various intercept trajectories depicted in Section 4.4. If the standard deviation in time-to-go, σ_{tgo}, is used as a measure of guidance performance, then the *performance* of the guidance algorithm does not vary dramatically for the different closing geometries examined. However, to achieve this performance, the *behavior* of the guidance algorithm does vary significantly for each of the different closing geometries. Behavior, in this case, refers to the magnitude of the velocity impulses computed by the guidance. This variation in behavior is illustrated by comparing the magnitude of the velocity impulses for the head-on and tail chase intercepts. In the former case, the magnitude of the first velocity impulse is about 1/4 that of the second. In the latter case, the magnitude of the first impulse is about 3 times that of the second. The results indicate that this variation in behavior is strongly dependent on the total time available for intercept.

Since the results for the different starting ranges were about the same for a given

Table 5.1. Initial Conditions that Remained Constant Throughout Performance Analysis

Burn times: $t_1 = 25\%\, t_f \quad t_2 = 50\%\, t_f \quad t_3 = 75\%\, t_f$
Variance factor: $f = 1 \times 10^{11}$
Angle measurement quality:
$\sigma_\theta = \sigma_\phi = 0.5 \times 10^{-4}$ rad/sec $\qquad \rho_{\theta\phi} = 0$
Initial quality of navigation filter state:
$\sigma_{r_x} = \sigma_{r_y} = \sigma_{r_z} = 5000$ ft
$\sigma_{v_x} = \sigma_{v_y} = \sigma_{v_z} = 5$ ft/sec
Cross-correlations all zero

bearing angle, only the performance results for the 1000 nm starting range are discussed. These will be referred to as the "1000 nm intercepts" in the following discussion. Before detailing the performance results, Table 5.1 summarizes the simulation inputs that remained constant throughout the entire performance analysis. Also, for completeness, the initial conditions specific to each of the 1000 nm intercepts is summarized in Appendix A . Table 5.2 contains a selection of values from this Appendix for reference in the following discussion. Note that the relative position and velocity vectors given in Table 5.2 are expressed in the xyz coordinate frame described in Section 4.3.1. The coordinate frame has been selected such that the initial position has only one non-zero component, r_x, and that the relative velocity has only two components, v_x and v_z. It is the z direction in which the maneuvers are applied. This

Table 5.2. Summary of Initial Conditions for Various 1000 nm Intercept Trajectories

Bearing Angles (degrees)	Intercept Time (sec)	Relative Position $(r_x,\ r_y,\ r_z)$ (ft)	Relative Velocity $(v_x,\ v_y,\ v_z)$ (ft/sec)	Burn Times (sec)
0	92	(3280840, 0, 0)	(-35354, 0, 59)	23 46 69
45	98	(3280840, 0, 0)	(-33111, 0, 66)	24 49 73
90	117	(3280840, 0, 0)	(-27853, 0, 90)	29 58 87
135	154	(3280840, 0, 0)	(-21002, 0, 145)	38 77 116
180	186	(3280840, 0, 0)	(-17402, 0, 195)	46 93 134

direction is subsequently referred to as the normal direction.

5.1 Variance in Time-to-go and the Velocity Corrections

Since the objective of the guidance is to minimize the cost, J, by trading variance in time-to-go for fuel usage, it is appropriate to first review the reduction in σ_{tgo} achieved and the maneuvers that produce the reduction. (Although cost function minimization was performed using the variance, the following discussion will refer to its square root, the standard deviation, since this value is more commonly quoted in practice.) Table 5.3 summarizes the uncertainty in time-to-go at three different points in the simulation. The third and fifth columns indicate the initial and final uncertainties in time-to-go based on the navigation filter estimate. The fourth column indicates the value of $\sigma_{tgo}(t_3)$ predicted by the guidance at the time of the first burn.

Table 5.3. Variance in Time-to-go at Different Times in the Trajectory

Intercept Time (sec)	t_3 (sec)	$\sigma_{tgo}(t_0)$ (msec)	$\tilde{\sigma}_{tgo}(t_3)$ (msec)	$\sigma_{tgo}(t_f)$ (msec)
92	69	142.0	16.0	12.6
98	73	150.7	15.9	12.0
117	87	180.7	15.5	11.5
154	116	240.9	14.7	11.7
186	139	292.3	14.4	11.3

These predicted values ($\tilde{\sigma}_{tgo}(t_3)$) are between 5 and 10 milliseconds smaller than the "actual" values ($\sigma_{tgo}(t_3)$, not shown in Table) obtained by the navigation filter at t_3. This is expected because the guidance does not model the periods during which no measurements are taken within the environment.

Also, with reference to Table 5.3, it should not be surprising that the value of σ_{tgo} achieved by the navigation filter at the end of the mission ($\sigma_{tgo}(t_f)$) is smaller than the value of σ_{tgo} predicted by the guidance for the time, t_3. This is because the navigation filter is able to take additional measurements between t_3 and t_f that the guidance can not. (The guidance prediction ends at t_3.)

As evident in the third column, the initial uncertainty in time-to-go increases as the intercept time increases. This is a result of the dependence of t_{go} on closing

velocity, the variation in which is shown by the relation

$$\mathrm{E}\{\delta t_{go}^2\} = \mathrm{E}\left\{\left(\frac{\delta r_c}{v_c}\right)^2\right\} + \mathrm{E}\left\{\left(\frac{r\ \delta v_c}{v_c^2}\right)^2\right\}$$

where r_c and v_c represent the position and velocity along the line-of-sight to the target and $\mathrm{E}\{\delta r_c\ \delta v_c\} = 0$. Despite the relatively large variation (150 msec) in initial uncertainty, $\sigma_{tgo}(t_0)$, the guidance brings the final uncertainty, $\sigma_{tgo}(t_f)$, to about the same value for all the intercept trajectories. The variation in the final value of σ_{tgo} is only 1.3 milliseconds. Even $\tilde{\sigma}_{tgo}(t_3)$ predicted by the guidance at the time of the first maneuver varies little (1.6 msec) for the different closing geometries.

Because the initial values of σ_{tgo} vary considerably but the final values do not, the amount of information gain between the initial time, t_0, and the final time, t_f, must also vary considerably. This is illustrated in Figures 5.1 through 5.5, which show the actual error and uncertainty in time-to-go as the mission proceeds. The uncertainty has been plotted both above and below the horizontal axis to indicate the "1-σ envelope" that typically encloses the actual error. Note that the initial value of the actual error (selected at random) happens to be quite small for the cases depicted in Figures 5.1 through 5.5. The same set of initial state errors were used for all trajectories.

It is interesting to note that the noisy measurements do not start to affect the actual error in t_{go} until the observability becomes significant. That is, the actual error remains almost unchanged until the variance in t_{go} begins to be reduced as a result of the maneuvers. Because the initial error is so small for these particular cases, it appears that the effect of the measurements is to increase, on average, the actual error

in the estimate. The truth in this seemingly ironic situation is that, in practice, one would not know that the initial errors happened to be unusually small in a particular case.

By comparing Figures 5.1 through 5.5, it is clear that a significant variation in the amount of information gained between velocity impulses exists for the various intercepts. In the 92 second intercept, a net reduction in uncertainty of approximately 130 milliseconds is realized (Figure 5.1). The majority of this reduction (85%) occurs between the second ($t = 46$ sec) and final impulse ($t = 69$ sec). Only a 4% reduction occurs between the first ($t = 23$ sec) and the second impulse. As the intercept time increases, the information gain between the first and second impulse becomes more significant. In the 186 second intercept, a net reduction of 281 milliseconds is realized with 59% of the reduction occurring between the first ($t = 46$ sec) and second ($t = 93$ sec) impulse, and only 35% occurring between the second and final ($t = 139$ sec) impulse (Figure 5.5). The factor actually causing this variation in information gain between intercept trajectories is the significant variation in velocity impulses determined by the guidance.

Table 5.4 summarizes the magnitude of the velocity impulses that were applied in each of the trajectories. All velocity impulses were applied in the normal direction. As the intercept time increases, the magnitude of the first velocity correction increases while the second decreases. In the 92 second intercept, the first velocity correction, 562 ft/sec, is roughly 1/4 that of the second, 2539 ft/sec. The ratio changes considerably for the 186 second intercept. Here the first impulse, 1620 ft/sec, is about 3 times

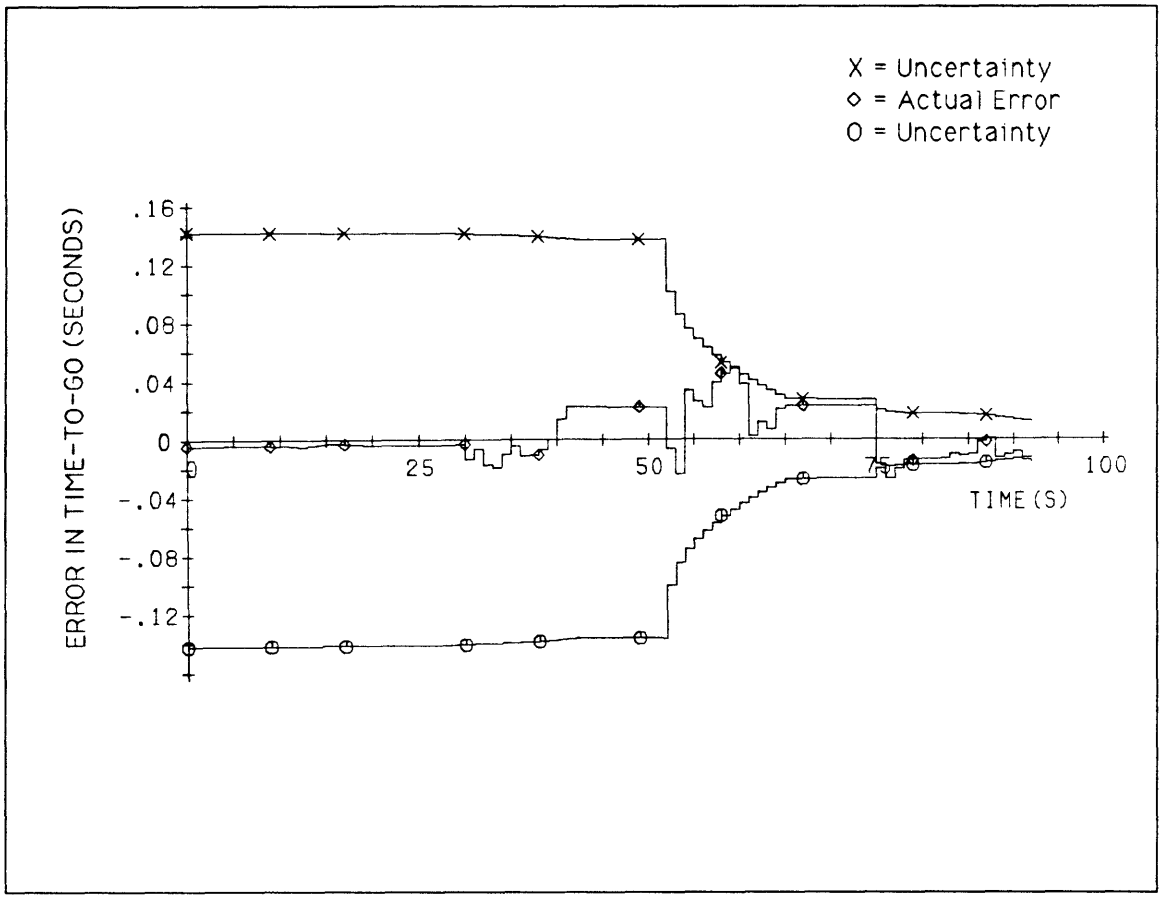

Figure 5.1. Actual Error and Uncertainty in Time-to-go for 92 Second Intercept

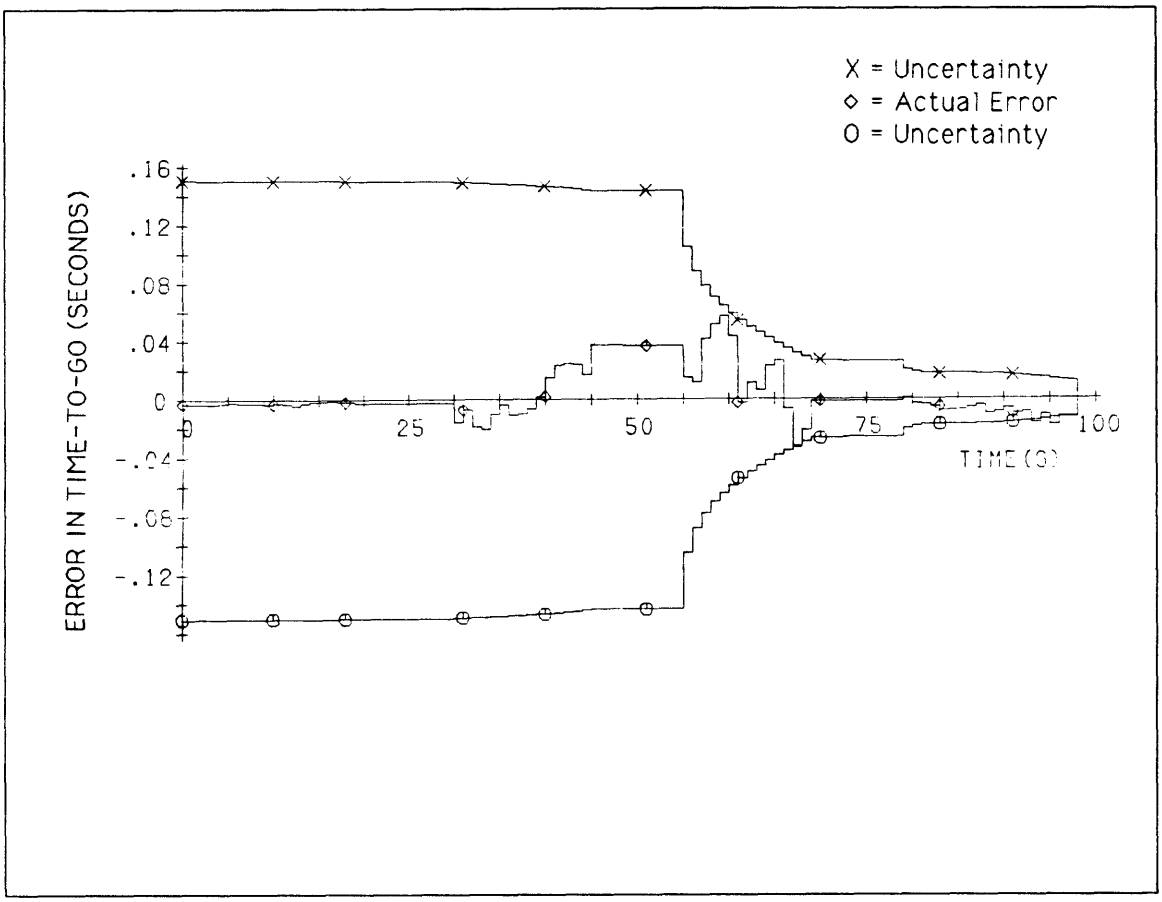

Figure 5.2. Actual Error and Uncertainty in Time-to-go for 98 Second Intercept

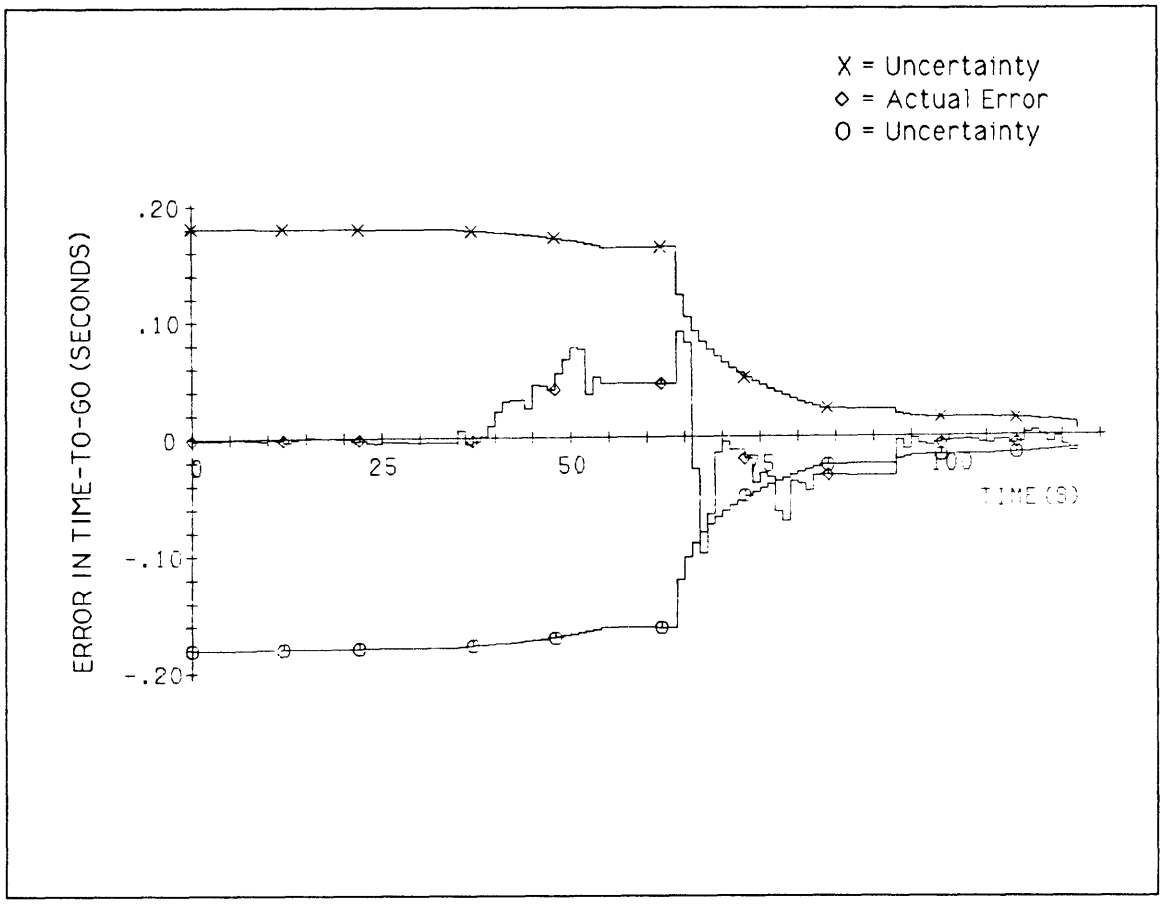

Figure 5.3. Actual Error and Uncertainty in Time-to-go for 117 Second Intercept

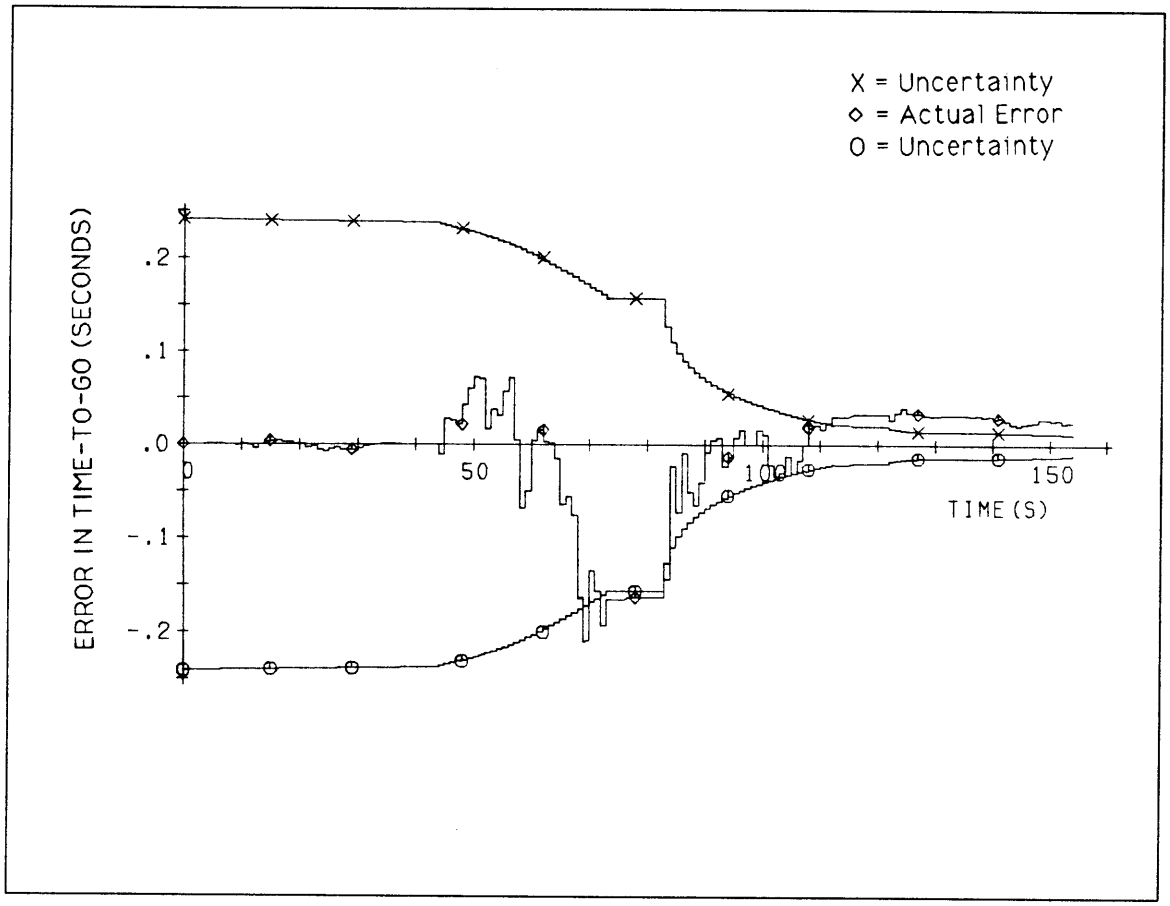

Figure 5.4. Actual Error and Uncertainty in Time-to-go for 154 Second Intercept

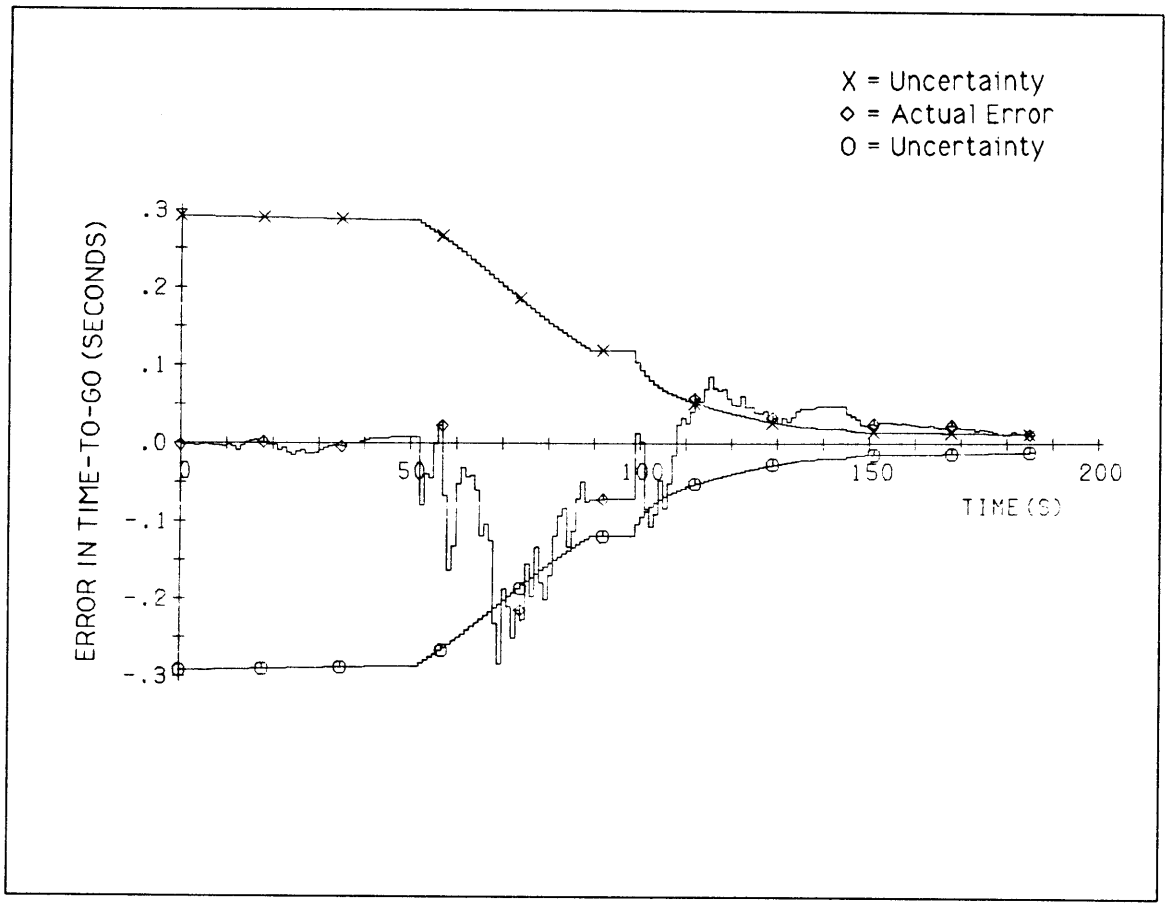

Figure 5.5. Actual Error and Uncertainty in Time-to-go for 186 Second Intercept

Table 5.4. Magnitude of the Velocity Impulses Applied

Intercept Time (sec)	ΔV_{1_z} (ft/sec)	ΔV_{2_z} (ft/sec)	$\lvert\Delta V_{hit}\rvert$ (ft/sec)	Total $\lvert\Delta V\rvert$ (ft/sec)
92	562	2539	6725	9826
98	585	2511	6678	9774
117	723	2215	6485	9423
154	1133	1316	6081	8530
186	1620	561	5955	8136

that of the second, 518 ft/sec. Accompanying this change in ratio is a reduction in $|\Delta V_{hit}|$ and $|\Delta V_{tot}|$. A reduction in $|\Delta V_{tot}|$ is not unexpected since a given velocity impulse has longer to 'act' (between burns) for the longer intercept times, causing the interceptor to travel further from the initial line-of-sight (for a given ΔV) and thereby, increasing position (σ_{tgo}) observability in the initial line-of-sight direction. The effect of these velocity corrections on the trajectories will be considered in Section 5.3.

Because the various intercept geometries differ (in a relative sense) only in closing and normal velocities at the start of each simulation (Table 5.2), only these two factors can contribute to the significant variations in ΔV_1 and ΔV_2 mentioned above. To determine which of these initial velocity components contributes most significantly to the variation in guidance behavior, two different guidance calls were made at the start of each simulation. The first call was a standard guidance call, returning the velocity corrections that minimize the cost, J. The second call was identical to the

Table 5.5. Velocity Corrections Predicted at the Start of the Simulation for both a Standard Guidance Call and a Guidance Call with a Nulled Normal Velocity

	Standard Guidance Call		Guidance Call w/nulled Out-of-plane Velocity	
Intercept Time (sec)	ΔV_{1_z} (ft/sec)	ΔV_{2_z} (ft/sec)	ΔV_{1_z} (ft/sec)	ΔV_{2_z} (ft/sec)
92	604	2418	656	2443
98	622	2392	684	2409
117	748	2097	826	2136
154	1125	1226	1275	1260
186	1574	482	1823	468

first, except that the initial normal velocity was set to 0. Since the position vector for all intercept trajectories is identical at the start of each simulation (Table 5.2), the resultant velocity corrections returned for the two different guidance calls indicate the effect of normal velocity on the optimal velocity corrections.

Table 5.5 summarizes the optimal velocity corrections found for both sets of simulations. The first and second column contain the velocity corrections for the standard guidance call, while the third and fourth column contain the velocity corrections for the non-standard guidance call. As shown in Table 5.5, the guidance call with the zeroed out-of-plane initial velocity returns velocity corrections similar to that of the standard guidance call. This indicates that the out-of-plane velocity has little effect on the optimal velocity corrections determined by the guidance. Thus, the variation in line-of-sight velocity associated with the different intercept trajectories is responsible for the variation in guidance behavior.

It is interesting to note that all of the first velocity corrections for the non-standard guidance call are slightly larger than those of the standard guidance call. In fact, the difference is approximately equal to the initial out-of-plane velocity (Table 5.2) that had been nulled out in the non-standard guidance call.

5.2 Navigation Filter Performance

Another measure of guidance performance is the reduction in state (position and velocity) uncertainty experienced by the navigation filter. It is these errors that indicate the expected final miss distances. For the following discussion the navigation uncertainties have been expressed in a current line-of-sight coordinate frame. The coordinate frame has one axis pointing in the current line-of-sight direction to the target. The other two directions are referred to as the horizontal and up directions. The horizontal direction is orthogonal to both the current line-of-sight direction and the current inertial position vector. The up direction is orthogonal to both the current line-of-sight and horizontal directions. In the following discussion, the horizontal and up directions are referred to as the normal directions.

5.2.1 Relative Position Uncertainty

Figures 5.6 through 5.11 summarize the navigation filters relative position error and uncertainty in both the line-of-sight and normal directions for the different intercept trajectories examined. For the normal directions, only the up position error for the 92 second intercept is shown since it is representative of the normal position uncertainties

for all of the closing trajectories examined.

As evident in Figures 5.6 through 5.10, the position uncertainty along the line-of-sight demonstrates the same behavior as the uncertainty in time-to-go. This is not unexpected since time-to-go is strongly dependent on the line-of-sight position. For the closing geometries with the shorter intercept time, the largest reduction in position uncertainty occurs between the second and final impulses. In the 92 second intercept, the position uncertainty is reduced by 4549 ft between the start of the simulation and the time of impact. The largest reduction, 85%, occurs between the second and third impulse. This is in contrast to the reduction in position uncertainty experienced in the 186 second intercept. Here, the uncertainty is reduced by 2795 ft, with only 35% occurring between the second and third impulses and 62% between the first and second. Just as for the uncertainty in time-to-go, the variation in the information gain between impulses for the different closing geometries is related to the velocity impulses computed by the guidance and applied by the environment program.

Although the line-of-sight position uncertainty was heavily influenced by the velocity corrections, the normal position uncertainties were not. As evident is Figure 5.11, the initial position uncertainty in the normal directions were rapidly reduced by the first few measurements. Indeed, 10 seconds into the mission the uncertainty was quickly reduced from 5000 ft to approximately 100 ft. From here, both normal position uncertainties ($1\sigma_{r_{normal}}$) progress slowly to their final values, with no dramatic changes resulting from the velocity corrections. In all trajectories, the final normal

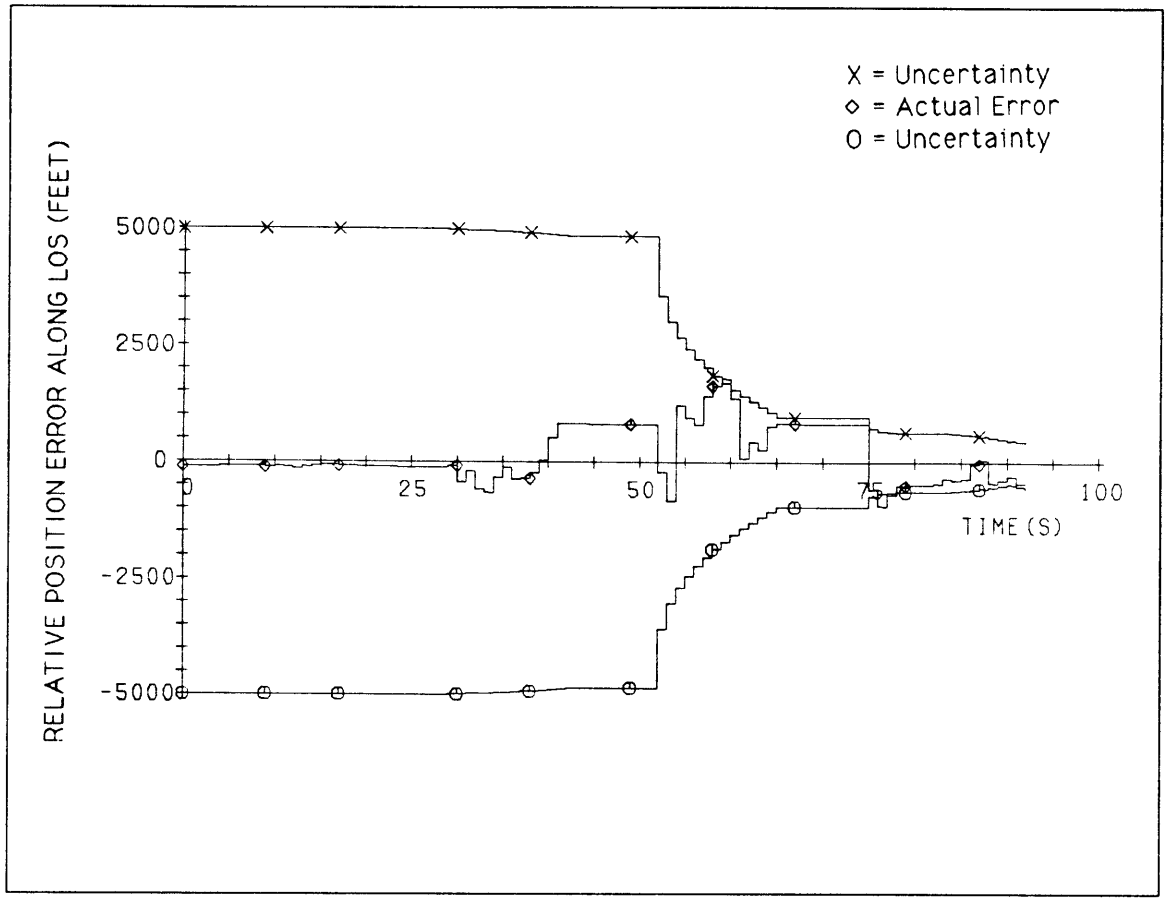

Figure 5.6. Relative Line-of-Sight Position Error and Uncertainty for 92 Second Intercept

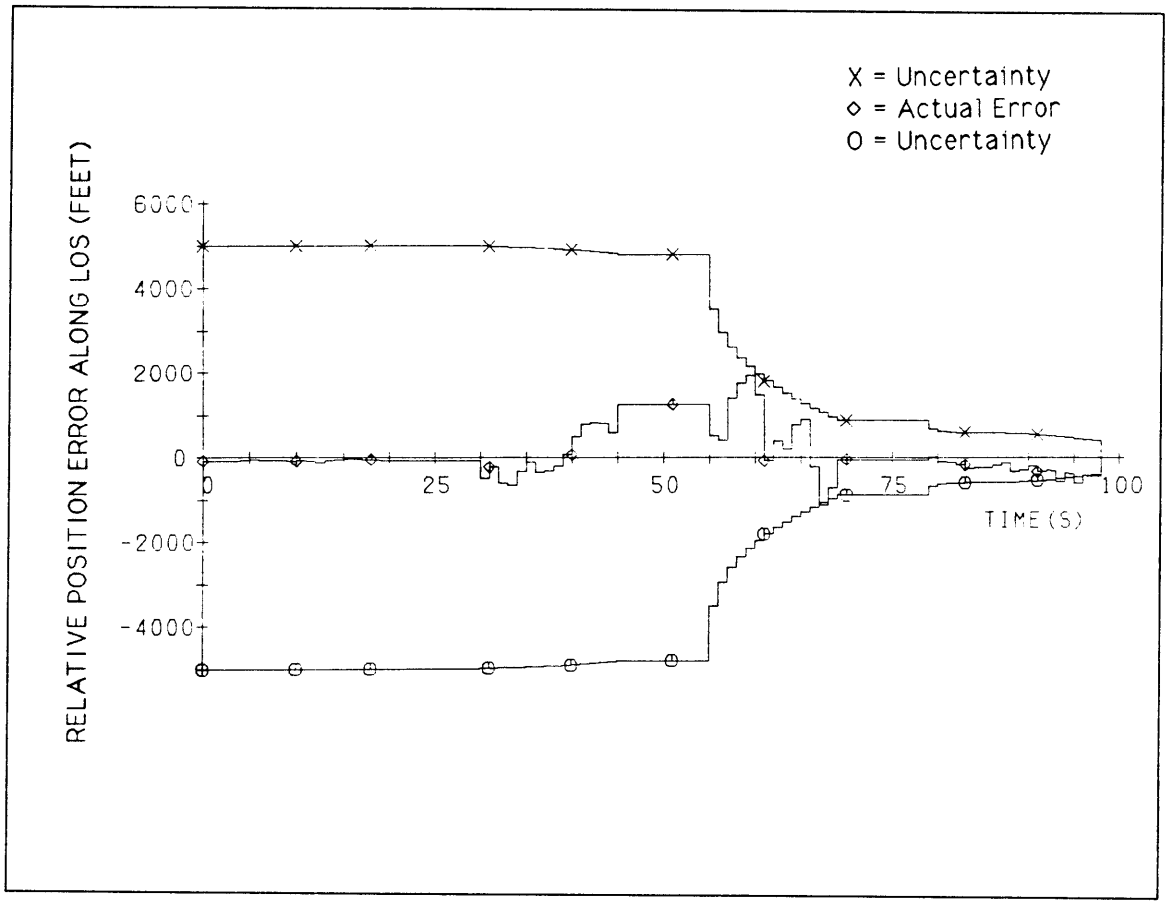

Figure 5.7. Relative Line-of-Sight Position Error and Uncertainty for 98 Second Intercept

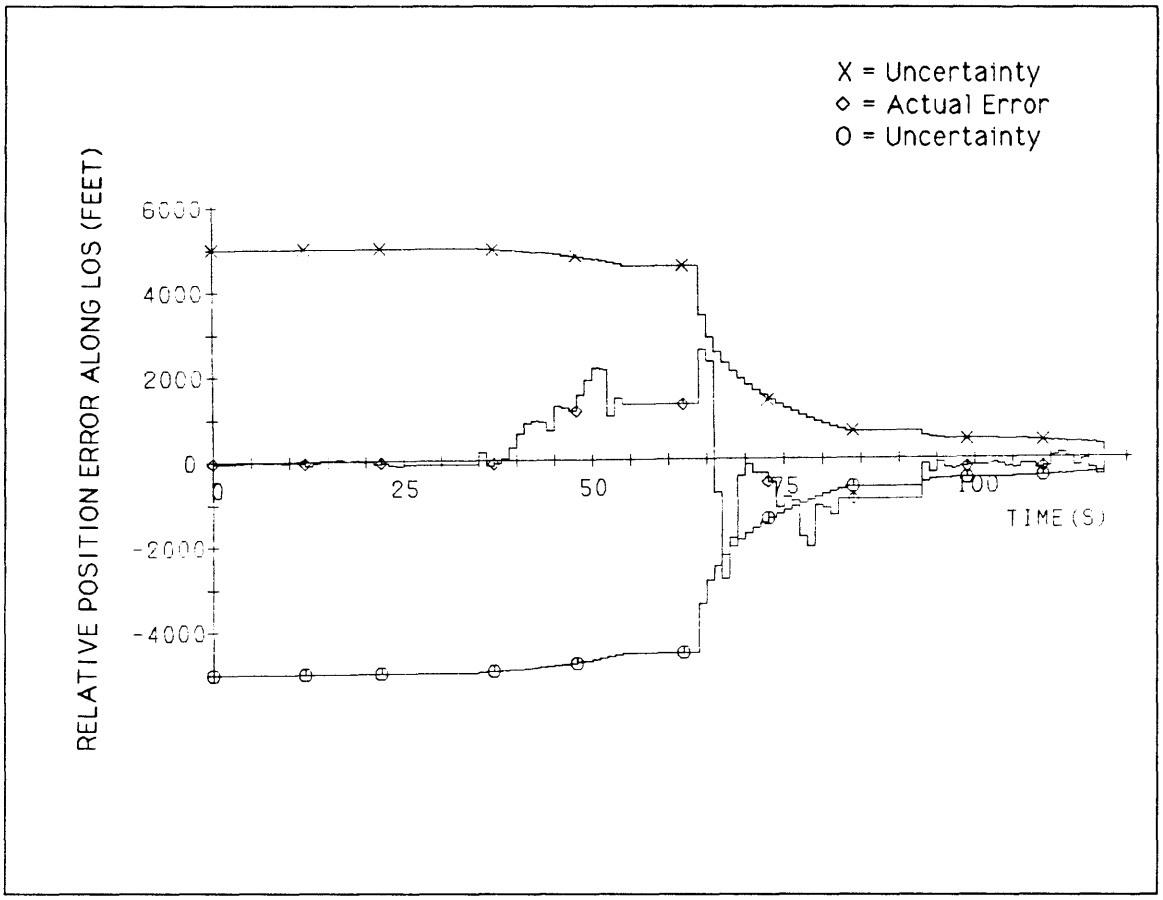

Figure 5.8. Relative Line-of-Sight Position Error and Uncertainty for 117 Second Intercept

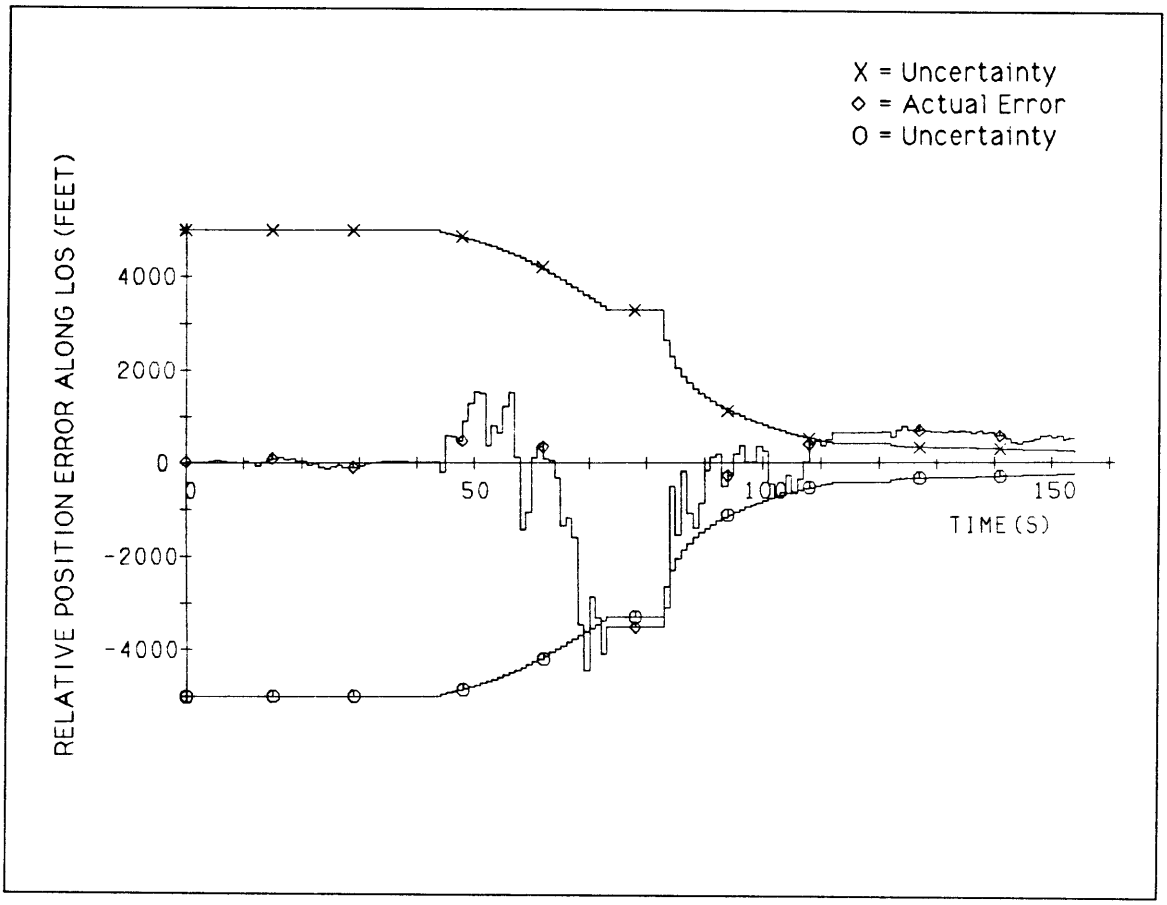

Figure 5.9. Relative Line-of-Sight Position Error and Uncertainty for 154 Second Intercept

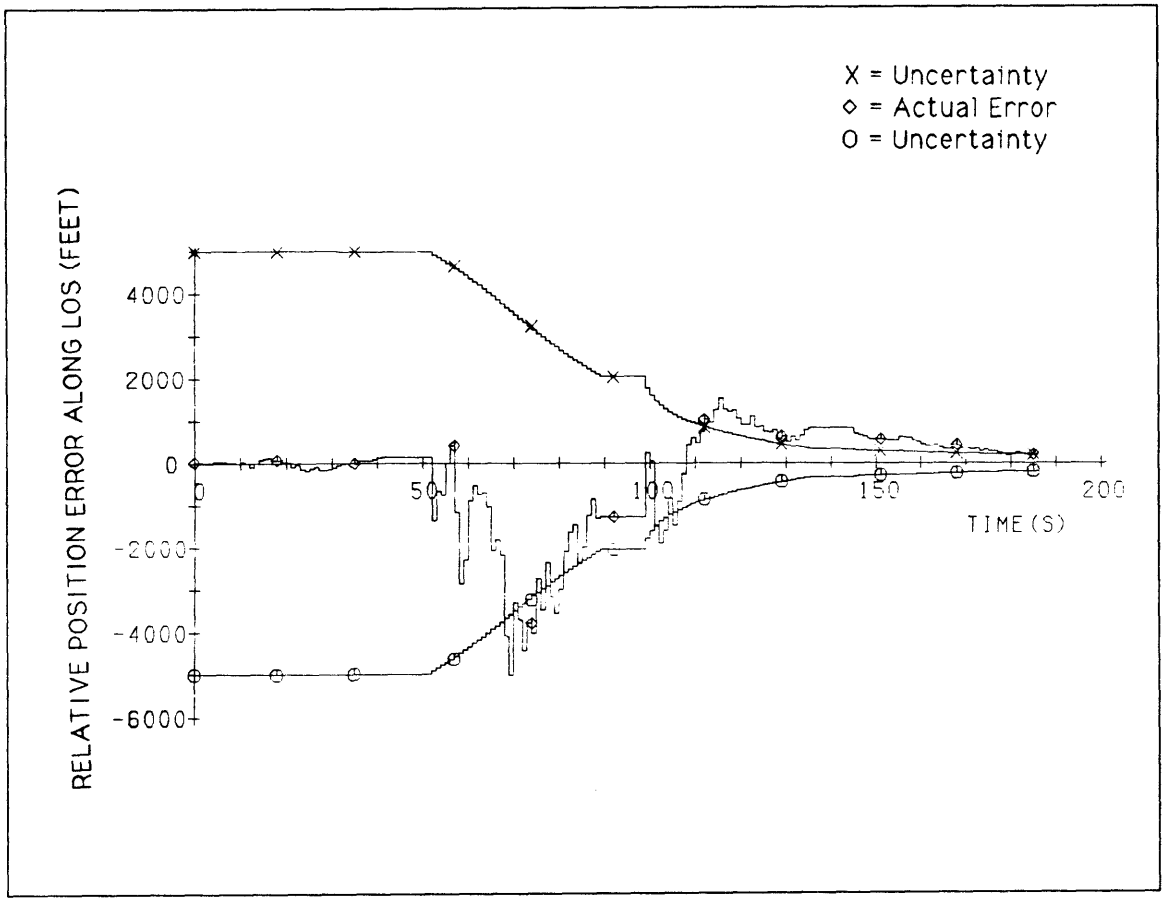

Figure 5.10. Relative Line-of-Sight Position Error and Uncertainty for 186 Second Intercept

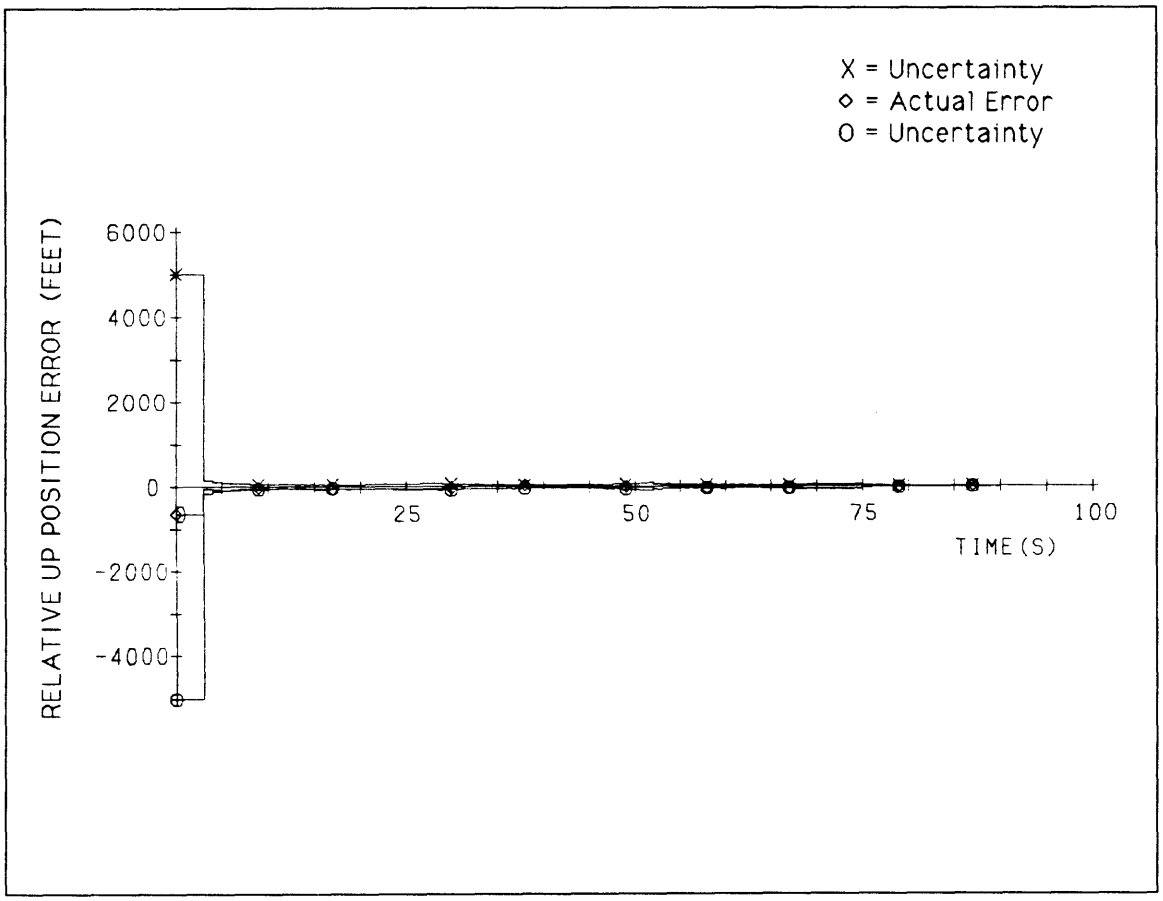

Figure 5.11. Relative Up Position Error and Uncertainty for 92 Second Intercept

position uncertainty fell below 6 feet. Under these modeling conditions, the contact expander would be designed to increase the area of contact by at least $3\sigma_{r_{normal}} = 18$ feet to guarantee a hit 99.4% of the time. The actual design size would also have to account for time-to-go uncertainty, which depends heavily on the line-of-sight position uncertainty and, to a lesser extent on the line-of-sight velocity uncertainty.

5.2.2 Relative Velocity Uncertainty

Figure 5.12 summarizes the relative velocity uncertainty and error in the line-of-sight direction for the 186 second intercept. This figure can be considered as representative of the velocity uncertainty for the other intercepts, with the only difference being the size of the reduction in uncertainty realized between the final maneuver and intercept. As indicated, there is essentially no reduction in relative velocity uncertainty between the start of the mission and the final maneuver. The majority of the reduction occurs after the hit maneuver, where the range is substantially reduced from its initial value. Table 5.6 summarizes the reduction in uncertainty between the final maneuver and intercept for the different closing geometries. The slower closing velocities associated with the longer intercept times allows the navigation filter more time to reduce the relative velocity uncertainty. In the 92 second intercept, the velocity uncertainty is reduced by 0.57 ft/sec while, in the 186 intercept, the velocity uncertainty is reduced by 3.49 ft/sec.

In contrast to the line-of-sight velocity uncertainties, the normal velocity uncertainties experience a moderate reduction even before any maneuvers are made. For this discussion, the relative velocity uncertainties in the two normal directions are

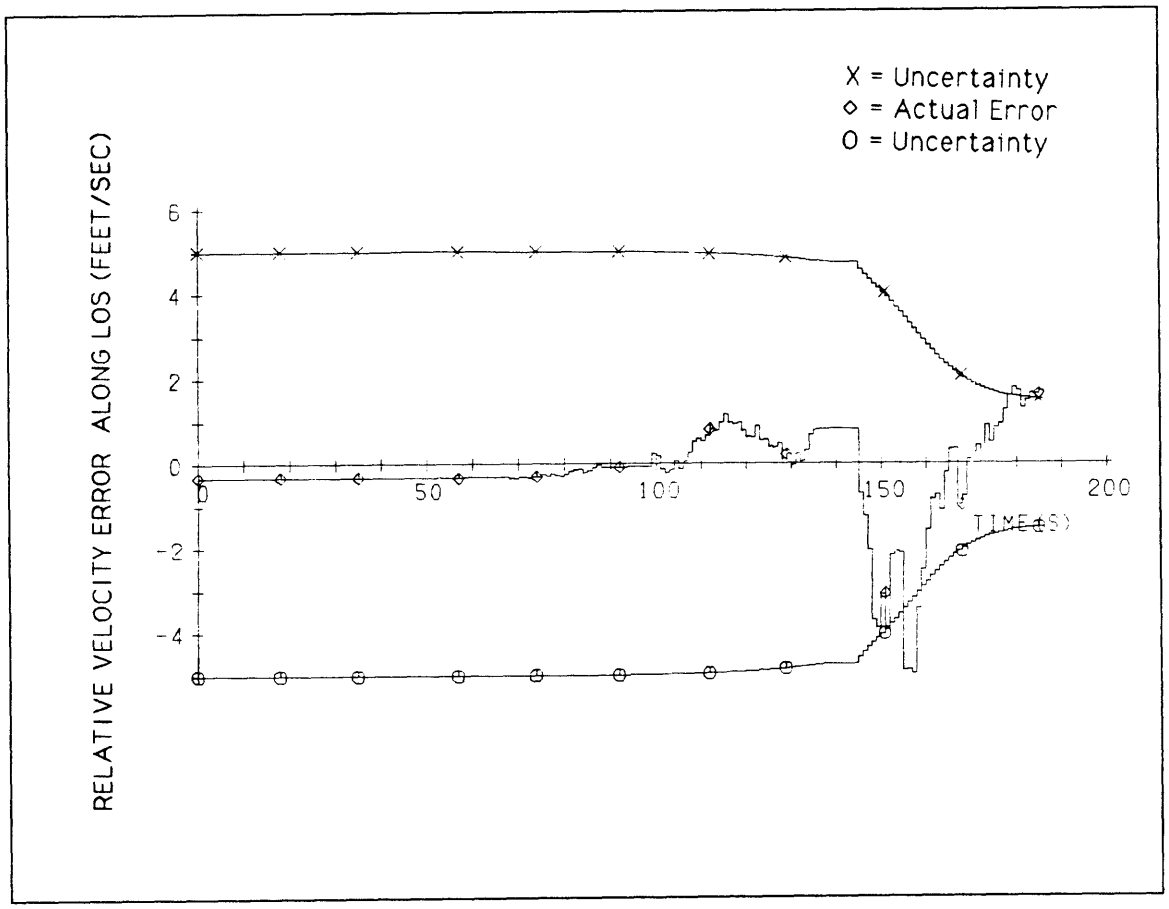

Figure 5.12. Relative Line-of-Sight Velocity Error and Uncertainty for 186 Second Intercept

Table 5.6. Reduction in Relative Velocity Uncertainty Between t_3 and t_f

Intercept Time (sec)	$\sigma_{v_{LOS}}(t_3)$ (ft/sec)	$\sigma_{v_{LOS}}(t_f)$ (ft/sec)	$\sigma_{v_{LOS}}(t_f) - \sigma_{v_{LOS}}(t_3)$ (ft/sec)
92	4.97	4.43	0.54
98	4.97	4.28	0.69
117	4.87	3.70	1.24
154	4.87	2.29	2.58
186	4.74	1.51	3.23

shown in Figure 5.13 and 5.14 for the 92 second intercept. As evident in these figures, the relative velocity uncertainty in both normal directions experiences a 1 ft/sec reduction before the first maneuver. Thus, without performing any maneuver, the velocity uncertainty decreases. Indeed, for the 186 second intercept, where the interceptor has more time to observe the target between maneuvers, a 3 ft/sec reduction in both normal directions occurs between the start of the mission and the first maneuver.

The effect of the first, and subsequent, maneuvers is to slightly reduce the velocity information gain in the up direction as compared to the horizontal direction. This is because the up direction is essentially the plane-of-action, that is, the plane containing the relative motion. (It is exactly the plane-of-action for the head-on and tail chase intercepts.) By the end of the simulation, the velocity uncertainty in the horizontal direction is about half that in the up direction. For all intercept trajectories, the final uncertainty in both normal directions fell below 0.8 ft/sec.

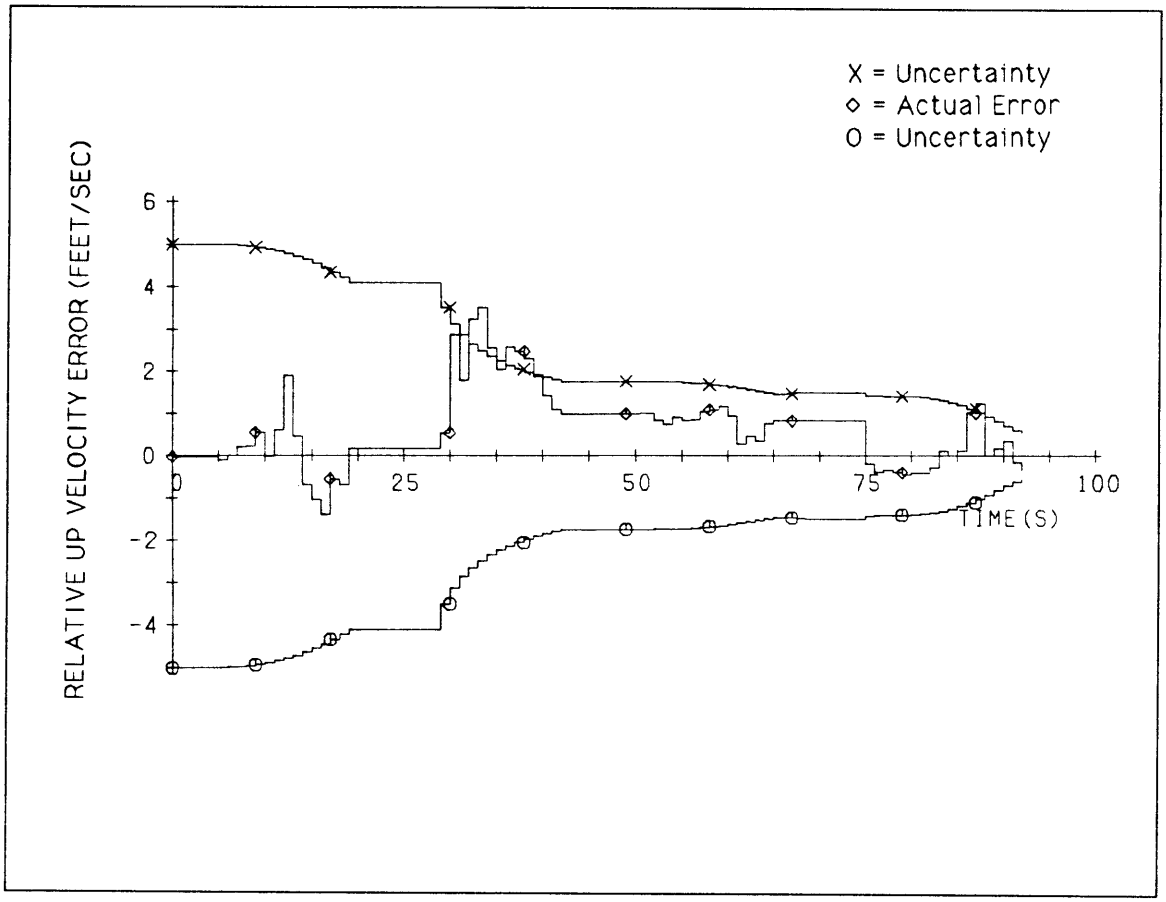

Figure 5.13. Relative Velocity Error and Uncertainty in Up Direction for 92 Second Intercept

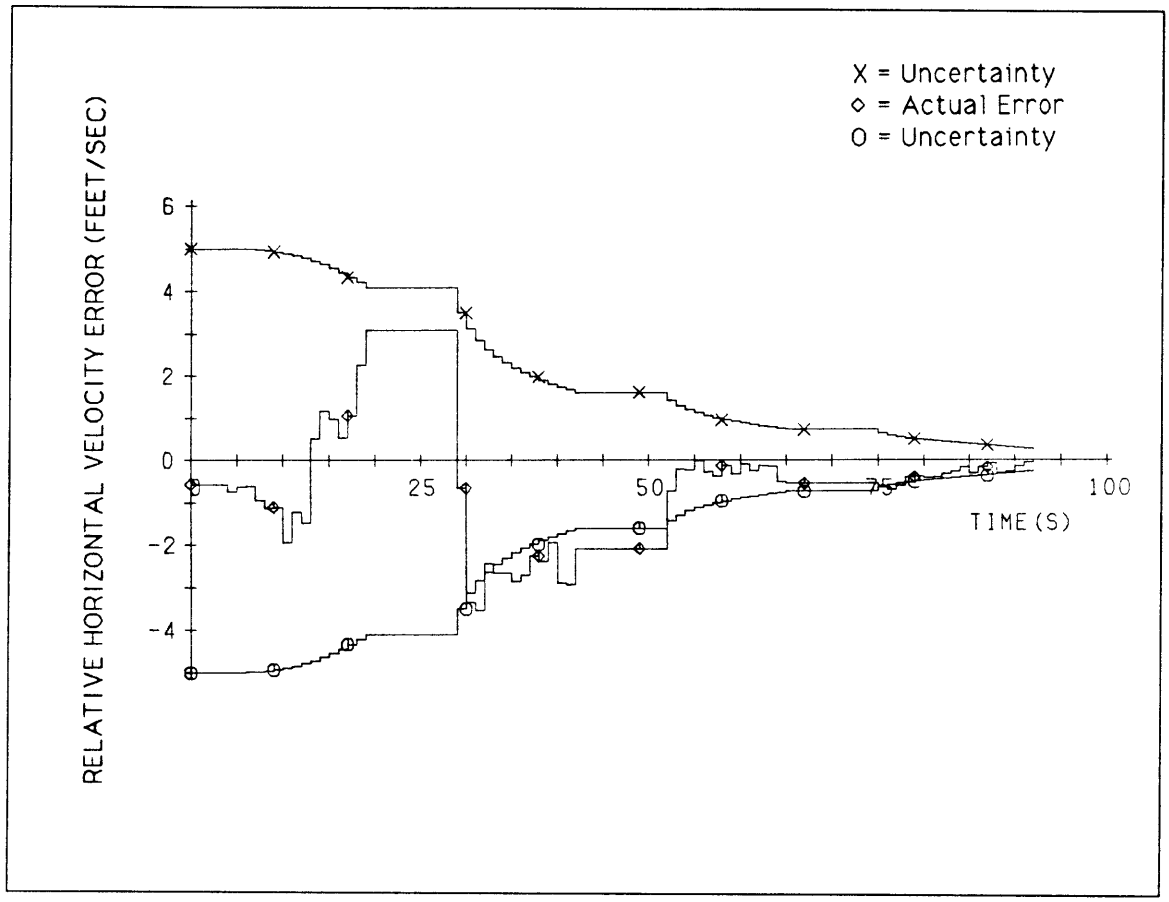

Figure 5.14. Relative Velocity Error and Uncertainty in Horizontal Direction for 92 Second Intercept

5.3 Relative Trajectories

Using the initial conditions of Table 5.2 and the velocity corrections of Table 5.4, the divert trajectory were reconstructed for each of the closing geometries. These trajectories[1] are illustrated in Figure 5.15, where position away from the initial line-of-sight has been plotted against percent of total mission time. The symbols indicate the points in the trajectory where the maneuvers were applied.

As evident, the shorter missions do not allow the interceptor to get as far away from the initial line-of-sight as the longer intercepts do. In the 92 second intercept, the interceptor gets approximately 80,000 feet off the initial line-of-sight, while in the 186 second intercept, the interceptor gets approximately 200,000 feet off the initial line-of-sight. The longer missions can afford, in terms of fuel cost, to get further away from the initial line-of-sight because the maneuvers have a longer period of time to "act". This is verified by the total fuel usage summarized back in Table 5.4. The 80,000 foot diversion for the 92 second intercept cost a total of 9,826 ft/sec, while the 200,000 foot diversion for the 186 second intercept cost only 8,136 ft/sec.

The actual trajectory represents a balance between two competing terms—fuel usage and variance in t_{go}. The fuel usage term attempts to keep the interceptor *close* to the initial line-of-sight, while the variance term attempts to take the interceptor *away* from the initial line-of-sight. The result of this competion in the shorter missions is to produce only a small trajectory deviation with the first maneuver and a large

[1]These trajectories were constructed assuming the gravitational acceleration acting on both vehicles was identical, giving linear motion.

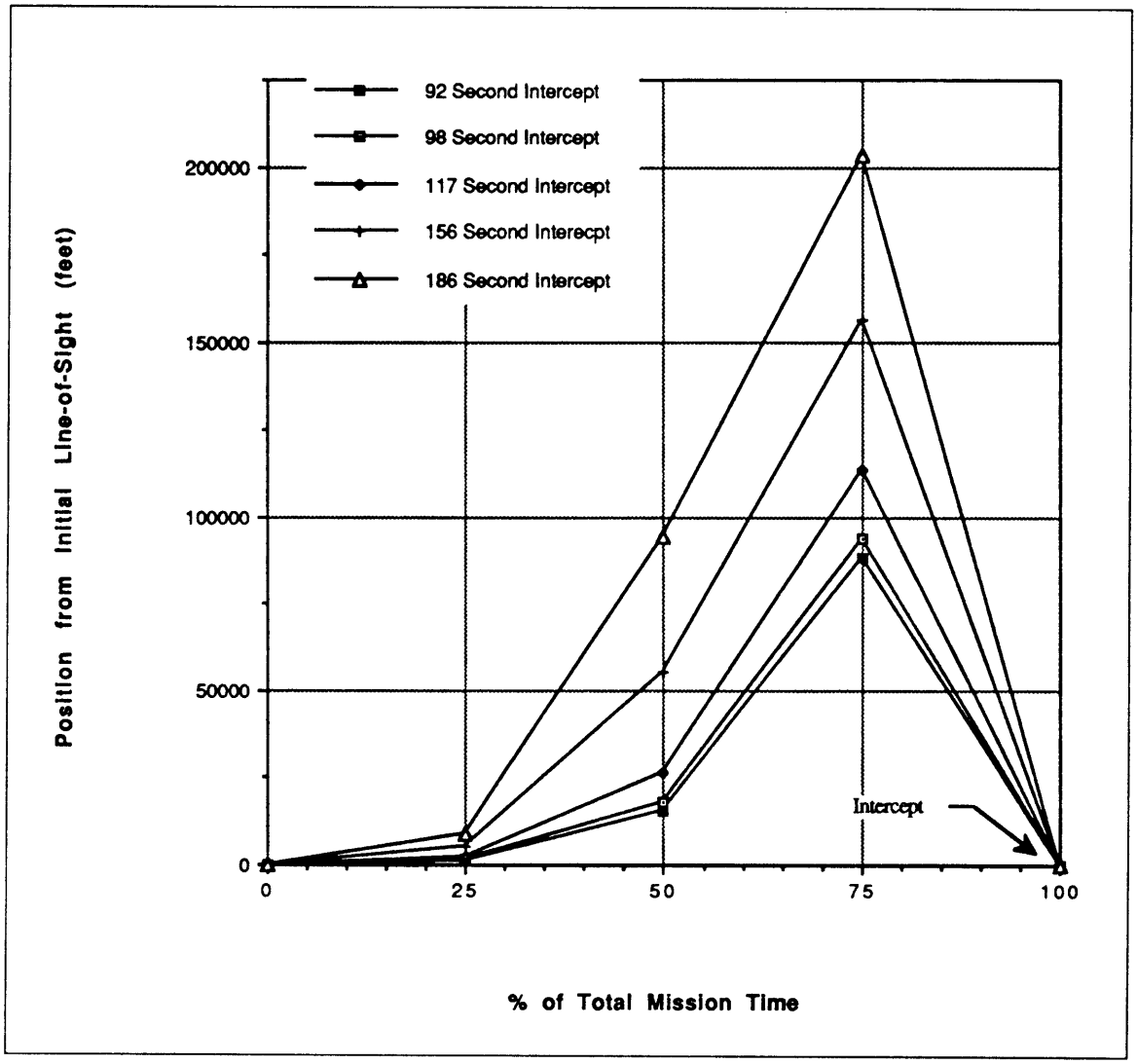

Figure 5.15. Trajectory Deviation from the Initial Line-of-Sight

deviation with the second maneuver. Based on the trends of Figure 5.15, an intercept significantly shorter than the 92 second mission shown would perform almost no divert from the initial line-of-sight until after the second maneuver. This is in contrast to the longer missions where the second maneuver adds only slightly to the divert produced by the first maneuver.

Chapter 6

Conclusions and Recommendations

The goal of this thesis has been to develop and study a long-range interceptor guidance algorithm for an interceptor that:

- takes angle-only measurements of the target, and
- performs only discrete maneuvers.

The guidance algorithm developed here links guidance trajectory selection to navigation filter performance. This forces the guidance algorithm to select a trajectory that both enhances the information content of the navigation filter and provides for target intercept. The resulting algorithm achieves this link through the minimization of a quadratic cost function composed of two terms. The first term provides a measure of navigation filter performance. The second term provides a measure of the fuel usage required to enhance the information content of the navigation filter.

The performance and behavior of this guidance algorithm was examined for several different target-interceptor closing geometries, ranging from head-on to tail chase. When σ_{tgo} is used as a measure of performance, the results indicate that the guidance reduces the final variance in time-to-go to about the same value for all of the intercepts—in spite of a large variation in the initial uncertainty in time-to-go for the different intercepts. However, when position and velocity uncertainties in the navigation filter are used as measures of performance, the longer missions tend to have a slightly lower state uncertainty at intercept than the shorter missions. This latter result is linked to the similar value of σ_{tgo} that the guidance achieves at intercept for all closing geometries.

Although the performance of the guidance algorithm did not vary significantly between closing geometries, the behavior did vary significantly. In the shorter missions, the first maneuver performed by the interceptor was quite small compared to the second maneuver. The second maneuver seemed to mark the start of any significant information gain by the navigation filter. In contrast, the first maneuver of the longer missions was substantially larger than the second maneuver. The navigation filter experienced a significant information gain as a result of the first maneuver, and only a moderate increase from the second maneuver.

Future research in this area might begin by exploring the behavior and performance of the guidance for different initial conditions than those listed in Table 5.1. Such variations would include decreased angle measurement accuracy. The value of noise, $\sigma_\theta = \sigma_\phi = 0.5 \times 10^{-4}$ rad/sec, chosen for this study represent good quality

angle measurements. Also, a variation in the burn times, such as 10%, 60%, and 80% may prove interesting. The results obtained in this study indicate that the largest information gain from the first measurement period occurred during the first few measurements (this is evident for the position uncertainties normal to the line-of-sight). Executing a maneuver soon after these first few measurements gives more time for the second maneuver to "act" and may, therefore, permit more effective utilization of the velocity corrections.

Future research in this area might also focus on releasing the restriction on impulses in the line-of-sight direction and, thus, allow changes in the time-to-go. A penalty for changes in time-to-go could be added to the cost function if a significant changes in time-to-go are not desired.

Unfortunately, the guidance algorithm developed here is not well suited for onboard implementation due to the dependence of the impulse magnitudes on closing velocity. This dependence prevents the construction of a single interceptor that can achieve the "ideal" performance (of the previous chapter) for all intercept geometries. It may still be possible to construct a single interceptor for a specific closing geometry (ie. the 90° bearing intercept), and still achieve acceptable performance for the remaining closing geometries. Perhaps a future study could determine the amount of degradation in σ_{tgo} incurred by such a design.

The guidance algorithm does lend itself well to preliminary design and trade-off studies. This algorithm provides a rigorous means of trading variance in time-to-go with fuel usage (and thus cost in dollars). Varying the weight factor on σ_{tgo}^2 allows

the guidance to adjust the relative cost between variance in t_{go} and fuel usage so that one may be emphasized more heavily than the other.

Finally, throughout the development of the guidance algorithm, it was taken for granted that performing two information-enhancing velocity corrections was better than performing only one. This was indeed verified in the analysis since both velocity corrections were non-zero for all intercept trajectories. This suggests that algorithms which consider the next velocity correction to be the last, as in Ref [3], would benefit by some knowledge of the existence of future velocity corrections.

Bibliography

[1] Speyer, J. L. and Hull, D. G., "Comparison of Several Extended Kalman Filter Formulations for Homing Missile Guidance," *Proceedings of the AIAA Guidance and Control Conference*, AIAA, New York, Aug. 1980, pp.392–398.

[2] Speyer, J. L., Hull, D. G., Tseng, C. Y., and Larson, S. W., "Estimation Enhancement by Trajectory Modulation for Homing Missiles," *Journal of Guidance, Control, and Dynamics*, Vol. 7, March-April, 1984, pp.167–174

[3] Casler, R. J. "A Dual-Control Guidance Strategy for Homing Interceptors Taking Angle-Only Measurements," Draper Laboratory Intralab Report.

[4] Friedland, B., *Control System Design: An Introduction to State-Space Methods*, McGraw-Hill Book Co., New York, 1986.

[5] Gelb, A., *Applied Optimal Estimation*, MIT Press, Massachusetts, 1989.

[6] Strang, G., *Introduction to Applied Mathematics*, Wellesley-Cambridge Press, Massachusetts, 1986.

[7] Battin, R. H., *Introduction to the Mathematics and Methods of Astrodynamics*, American Institute of Aeronautics and Astronautics, Inc., New York, N.Y. 1987.

[8] Battin, R. H., *Astronautical Guidance*, McGraw-Hill, Inc., New York, N.Y. 1964.

Appendix A

Summary of Initial Conditions Specific to Each Intercept

Tables A.1 through A.5 summarize the initial conditions that are specific to each of the 1000 nm intercepts. See Section 4.4 for further discussion concerning the procedure used to obtain these state vectors. Included in the following tables are the inertial state (position and velocity), the relative state, and the burn times.

Table A.1. Initial Conditions for 92 Second Intercept Trajectory

Target State			
$\vec{r}_t$	=	(21738816 -3782524 -2011203)	ft
$\vec{v}_t$	=	(4781 22286 11850)	ft/sec
Interceptor State			
$\vec{r}_i$	=	(22617521 -991545 -527214)	ft
$\vec{v}_i$	=	(-4744 -7774 -4133)	ft/sec
Relative State			
$\vec{r}$	=	(3280840 0 0)	ft
$\vec{v}$	=	(-35354 0 59)	ft/sec

Hit Time: $t_f = 92.8$ sec

Burn Times: $t_1 = 23$ $t_2 = 46$ $t_3 = 69$ sec

Table A.2. Initial Conditions for 98 Second Intercept Trajectory

Target State			
$\vec{r}_t$	=	(21711724 -3906689 -2077223)	ft
$\vec{v}_t$	=	(4938 22259 11835)	ft/sec
Interceptor State			
$\vec{r}_i$	=	(22620475 -1481008 -63729)	ft
$\vec{v}_i$	=	(-4358 -2369 -8611)	ft/sec
Relative State			
$\vec{r}$	=	(3280840 0 0)	ft
$\vec{v}$	=	(-33311 0 66)	ft/sec

Hit Time: $t_f = 98.1$ sec

Burn Times: $t_1 = 24$ $t_2 = 49$ $t_3 = 73$ sec

Table A.3. Initial Conditions for 117 Second Intercept Trajectory

Target State			
$\vec{r}_t$	=	(21612158 -4331407 -2303050)	ft
$\vec{v}_t$	=	(5474 22157 11781)	ft/sec
Interceptor State			
$\vec{r}_i$	=	(22632320 -2254878 23149)	ft
$\vec{v}_i$	=	(-3272 4551 -7950)	ft/sec
Relative State			
$\vec{r}$	=	(3280840 0 0)	ft
$\vec{v}$	=	(-27853 0 90)	ft/sec
Hit Time: $t_f = 117.2$ sec			
Burn Times: $t_1 = 29$ $t_2 = 58$ $t_3 = 87$ sec			

Table A.4. Initial Conditions for 154 Second Intercept Trajectory

Target State			
$\vec{r}_t$	=	(21385782 -5163212 -2745328)	ft
$\vec{v}_t$	=	(6523 21926 11658)	ft/sec
Interceptor State			
$\vec{r}_i$	=	(22648864 -3114295 -515873)	ft
$\vec{v}_i$	=	(-1696 8855 -2579)	ft/sec
Relative State			
$\vec{r}$	=	(3280840 0 0)	ft
$\vec{v}$	=	(-21002 0 145)	ft/sec
Hit Time: $t_f = 154{,}9$ sec			
Burn Times: $t_1 = 38$ $t_2 = 77$ $t_3 = 116$ sec			

Table A.5. Initial Conditions for 186 Second Intercept Trajectory

Target State			
$\vec{r}_t$	=	(21166771 -5850092 -3110549)	ft
$\vec{v}_t$	=	(7388 21702 11539)	ft/sec
Interceptor State			
$\vec{r}_i$	=	(22645453 -3264184 -1735597)	ft
$\vec{v}_i$	=	(-629 8063 4287)	ft/sec
Relative State			
$\vec{r}$	=	(3280840 0 0)	ft
$\vec{v}$	=	(-17402 0 195)	ft/sec

Hit Time: $t_f = 186.4$ sec

Burn Times: $t_1 = 46$ $t_2 = 93$ $t_3 = 139$ sec